esa

ECOSPHERE

Linking rainforest ecophysiology and microclimate through fusion of airborne LiDAR and hyperspectral imagery

EBEN N. BROADBENT,[1,2,3,7,]† ANGÉLICA M. ALMEYDA ZAMBRANO,[1,3,4,7] GREGORY P. ASNER,[1] CHRISTOPHER B. FIELD,[1] BRAD E. ROSENHEIM,[5] TY KENNEDY-BOWDOIN,[1] DAVID E. KNAPP,[1] DAVID BURKE,[1,2] CHRISTIAN GIARDINA,[6] AND SUSAN CORDELL[6]

[1]*Department of Global Ecology, Carnegie Institution, 260 Panama Street, Stanford, California 94305 USA*
[2]*Department of Biology, Stanford University, Stanford, California 94305 USA*
[3]*Sustainability Science Program, Kennedy School of Government, Harvard University, Cambridge, Massachusetts 02138 USA*
[4]*Department of Anthropology, Stanford University, Stanford, California 94305 USA*
[5]*Department of Earth & Environmental Sciences, Tulane University, New Orleans, Louisiana 70118 USA*
[6]*Institute of Pacific Islands Forestry, Hilo, Hawaii 96720 USA*

Citation: Broadbent, E. N., A. M. Almeyda Zambrano, G. P. Asner, C. B. Field, B. E. Rosenheim, T. Kennedy-Bowdoin, D. E. Knapp, D. Burke, C. Giardina, and S. Cordell. 2014. Linking rainforest ecophysiology and microclimate through fusion of airborne LiDAR and hyperspectral imagery. Ecosphere 5(5):57. http://dx.doi.org/10.1890/ES13-00255.1

Abstract. We develop and validate a high-resolution three-dimensional model of light and air temperature for a tropical forest interior in Hawaii along an elevation gradient varying greatly in structure but maintaining a consistent species composition. Our microclimate models integrate high-resolution airborne waveform light detection and ranging data (LiDAR) and hyperspectral imagery with detailed microclimate measurements. We then use modeled microclimate and forest structural and compositional variables to explain variation in spatially explicit measurements of leaf traits, including gas exchange and structure. Our results highlight the importance of: (1) species differences in leaf traits, with species explaining up to 65% of the variation in some leaf traits; (2) differences between exotic and native species, with exotic species having greater maximum rates of assimilation and foliar $\delta^{15}N$ values; (3) structural factors, with foliar %N and light saturation of photosynthesis decreasing in mid-canopy locations; (4) microclimate factors, with foliar %N and light saturation increasing with growth environment illumination; and (5) decreases in mean annual temperature with elevation resulting in closure of the nitrogen cycle, as indicated through decreases in foliar $\delta^{15}N$ values. The dominant overstory species (*Metrosideros polymorpha*) did not show plasticity in photosynthetic capacity, whereas the dominant understory species (*Cibotium glaucum*) had higher maximum rates of assimilation in more illuminated growth environments. The approach developed in this study highlights the potential of new airborne sensors to quantify forest productivity at spatial and temporal scales not previously possible. Our results provide insight into the function of a Hawaiian forest dominated by native species undergoing simultaneous biological invasion and climatic change.

Key words: canopy structure; Carnegie Airborne Observatory; climate change; direct and diffuse light; induction rate; Laupahoehoe Natural Area Reserve; photosynthetic active radiation (PAR); sun fleck; tropical forest.

Received 14 August 2013; revised 5 February 2014; accepted 12 March 2014; **published** 16 May 2014. Corresponding Editor: D. P. C. Peters.

[7] Present address: Department of Geography, University of Alabama, Tuscaloosa, Alabama 35487 USA.

† **E-mail:** eben@amazonico.org

Introduction

Tropical forests cover 11.7% of the global land surface area (Potter et al. 1993), contain 57% of above- and 27% of belowground carbon (Dixon et al. 1994), and are important contributors to the terrestrial global carbon cycle (Field et al. 1998, Cramer et al. 2004). Carbon fluxes and overall productivity within these forests are highly dependent upon light and temperature regimes (Boisvenue and Running 2006), which are predicted to undergo changes in the future (Hulme and Viner 1998, Mercado et al. 2009, Hansen et al. 2010). Light within a forest understory is considered to be the most important (Mercado et al. 2009), and limiting (Stadt et al. 2005), environmental factor influencing photosynthesis and carbon gain (Ellsworth and Reich 1992, Kull 2002, Araujo et al. 2008). Overall, light penetration to a tropical forest understory is among the lowest of terrestrial ecosystems (Chazdon and Pearcy 1991). The light which does exist is temporally variable, due to time of day, season or climatic conditions, and is highly dependent on the structure and density of both the forest under- and over-story (Montgomery 2004). Despite light limitation, the understory can make substantial contributions to overall forest productivity. For example, Sampson et al. (2006) calculated understory plants contributed up to 28% of a deciduous forest's gross primary productivity due to understory penetration by diffuse radiation.

Variation in microclimate often results in predictable changes in leaf traits (Poorter et al. 2006). The established paradigm is that photosynthesis is N limited (Evans 1989), and numerous studies have shown the significant positive relationship between leaf N content and maximum photosynthesis capacity (A_{max}) (Chazdon and Field 1987, Evans 1989, Evans and Poorter 2001), independent of species differences (Walters and Field 1987). Given this, forest canopies should optimize both the distribution of their leaves for high light capture efficiency and leaf photosynthetic rates according to their irradiance growth environment (Field 1983, Meir et al. 2002, Laisk et al. 2005). Canopy optimization of N distribution and photosynthetic capacity to light availability has been shown within a variety of crop and forest stands (Hirose et al. 1989, Hollinger 1989, Ellsworth and Reich 1993, Dang et al. 1997).

It remains unclear, however, how foliar acclimation and development adjusts to differing types and variability of irradiance (Meir et al. 2002, Bai et al. 2008). This is especially relevant when considering communities of diverse species, although the importance of such differences has been demonstrated (Chazdon and Field 1987). Understanding drivers of leaf trait variation in different species or functional groups (Poorter et al. 2006) is especially relevant in taxonomically and architecturally diverse, but light limited, tropical forest understory environments. A number of factors diminish the strength of relationships between light availability and investment in photosynthetic capacity, including light saturation, partitioning of nitrogen for non-photosynthesis activities, leaf aging, and position (Field 1983), or variation in temperature, wind speed, precipitation and nutrient availability, as well as species differences (Dang et al. 1997).

Ecosystem processes within tropical forests, such as overall productivity (Baldocchi and Harley 1995), occur within a complex three-dimensional architecture (Koetz et al. 2007). Interactions between architecture and microclimate require further study (Gastellu-Etchegorry and Trichon 1998). Failure to include spatial data on forest architecture, for example, can result in large errors from simple big-leaf models (Baldocchi and Harley 1995, Knohl and Baldocchi 2008). Attempts to estimate daily light regimes using traditional methods, such as hemispherical photographs, have resulted in inaccurate values, up to 107% greater than those shown from understory photosynthetic active radiation (PAR) sensors (Johnson and Smith 2006). Light regime modeling approaches explicitly integrating manually collected leaf area distributions showed greatly improved results (Aubin et al. 2000, Gersonde et al. 2004).

High-resolution light detection and ranging (LiDAR) sensors allow incorporation of spatially explicit information into microclimate models at scales infeasible through field data collection. Airborne LiDAR has recently been used to accurately estimate forest height (Hudak et al. 2002, Sexton et al. 2009, Dubayah et al. 2010), biomass (Asner et al. 2008*a*, Boudreau et al. 2008, Asner et al. 2012, Meyer et al. 2013), and

architecture (Omasa et al. 2007), including gap dynamics (Koukoulas and Blackburn 2004, Kellner and Asner 2009). The capacity to quantify forest structure over large areas at high resolutions has led to insights into ecosystem function (Asner et al. 2008*a*, *b*), including patterns of canopy height heterogeneity not visible at smaller scales (Vitousek et al. 2009). Discrete LiDAR, in which a small number of individual laser pulses are used (Lim et al. 2003), has more recently, been combined with hyperspectral imagery and used to generate maps of leaf chlorophyll (Thomas et al. 2006), providing insights into flux tower measurements of gross ecosystem productivity (Thomas et al. 2009). Waveform LiDAR (i.e., wLiDAR) differs from discrete LiDAR sensors as it records a higher point cloud per area, approximating the complete waveform of the backscattered echo signal (Mallet and Bretar 2009), allowing more accurate estimations of forest understory architecture (Asner et al. 2007). This could lead to a better understanding of forest productivity if data approximates the fine scales at which canopy microclimate and ecophysiology are determined, but comes at the expense of greatly increased storage capacity and subsequent post-processing requirements (Mallet and Bretar 2009). Parker et al. (2001) used wLiDAR, one of the first attempts integrating this technology, to estimate nadir light transmittance statistics for two forest stands; however, a horizontal resolution of 10 m made detailed forest interior studies infeasible. Koetz et al. (2006) used physically-based radiative transfer models to invert large footprint waveform LiDAR (wLiDAR) accurately estimating forest biophysical parameters, including leaf area index (LAI), tree height, and general interior forest architecture.

In this research, we develop a new approach to map forest leaf area (2D) and leaf density (3D) at very high spatial scales. Using these maps, we develop and validate a three-dimensional model of direct and diffuse light transmittance and air temperature throughout a tropical rainforest in Hawaii. We then couple the microclimate models with detailed spatially explicit measurements of plant ecophysiological characteristics across a community of native and invasive species to understand structural, taxonomic, and climatic determinants of ecophysiological properties. The selected study forest, a model ecosystem having a near mono-dominant canopy species and both invasive and native species coupled with an extraordinary elevation gradient along the slope of Mauna Kea volcano, enables addressing questions related to relationships among forest structure, climate and ecophysiology not feasible in other systems. The specific research objectives of this study are to: (1) develop and validate a high resolution three-dimensional model of forest microclimate using a coupled airborne LiDAR–hyperspectral sensor; and then to (2) integrate remote sensing information and modeled microclimate data to better understand the taxonomic, structural and microclimatic determinants of foliar ecophysiology in our study area.

Materials and Methods

Study design

Fig. 1 presents the overall study design, and we describe in detail each component of the flowchart below. We combined airborne remote sensing data with spatially explicit measurements of forest microclimate and ecophysiology. We then developed detailed spatio-temporal models of microclimate and used these models to understand variation in foliar ecophysiology. We parameterized and validated remote sensing and modeling components using extensive field data.

Study site

This study was undertaken in the 5,016 ha State of Hawaii Hilo Forest Reserve and Laupahoehoe Natural Area Reserve, designated as a Hawaii Experimental Tropical Forest (HETF) of the US Forest Service (USFS), located on the North Hilo coast of the island of Hawai'i, Hawai'i. This reserve is also the location of a newly established Hawaii Permanent Plot Network (HIPPNET) and Center for Tropical Forest Science (CTFS) research plot (www.ctfs.si.edu). The reserve encompasses an elevation gradient from 600 to 1800 m elevation, with overall gradients in temperature and precipitation of 13–18°C and 2000–3500 mm, respectively (Giambelluca et al. 2011). A 2.5 km long by 800 m wide study transect was established in the northern central portion of the reserve extending from 1005 to 1343 m elevation (Fig. 2), corresponding

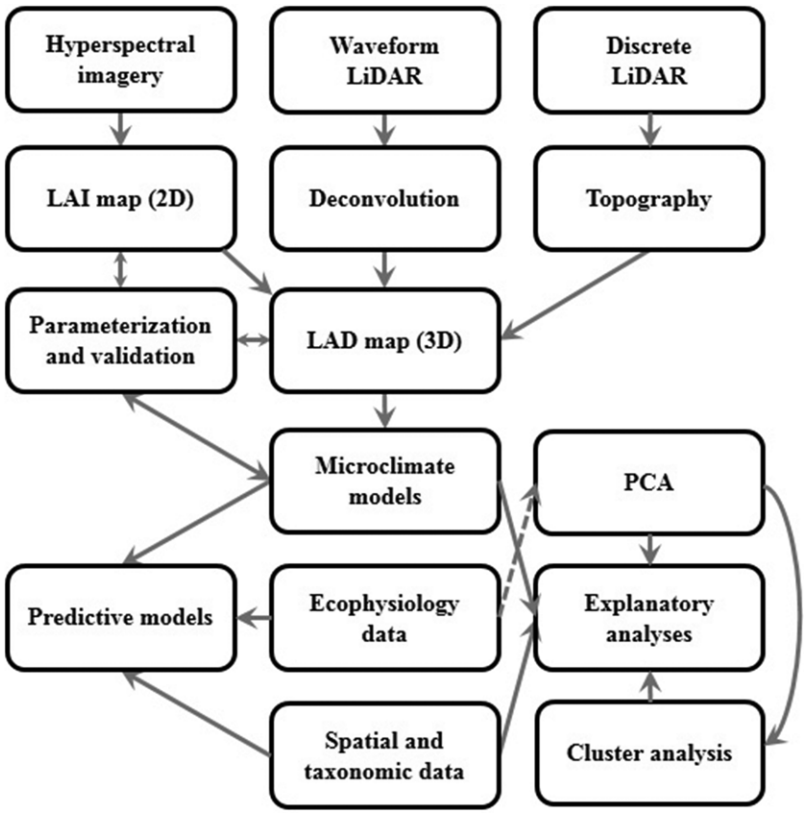

Fig. 1. Overview of remote sensing and field data integration and analysis. Hyperspectral and waveform light detection and ranging (LiDAR) data were collected simultaneously using the Carnegie Airborne Observatory (CAO) while discrete LiDAR was collected separately. Field data collected for parameterization and validation included: (1) LAI-2000 for leaf area index (LAI; two-dimensional), (2) vertical leaf area density (LAD; three-dimensional) transects, (3) microclimatic data, and (4) leaf trait measurements throughout the study transect. Leaf traits included chemical and gas exchange analyses. Microclimate data included modeled daytime mean and standard deviation photosynthetic photon flux density (PPFD) and modeled mean daytime air temperature. Spatial data included location, elevation, and forest structural information. Taxonomic data included species, native vs. exotic status, and life form. Principal component analysis (PCA) axes were input into *K*-means analysis to identify ecophysiological similar clusters that were explained through differences in microclimate, taxonomy, and spatial location.

to a mean annual temperature of 16.2–17.5°C, respectively, comparable to the projected increases in global temperature over the next century (Nozawa et al. 2001). While three distinct substrate ages exist within the reserve: 4–14, 14–25 and 25–65 ty (ty = 1000 yrs.), resulting from previous lava flows, the study transect was located entirely on youngest flow (4–14 ty). The transect consisted of two soil types, the lower half resting on the Akaka soil (rAK) and the upper half on Honokaa silty clay loam (HTD), both considered well drained with moderate available water capacity (websoilsurvey.nrcs.usda.gov, accessed 06/02/2011). The study transect was situated to keep the native Hawaiian tree *Metrosideros polymorpha* v. *glaberrima* (Myrtaceae) constant as the dominant canopy species, to the near exclusion of all others. Aboveground biomass (AGB) across the study transect ranged from approximately 500 $Mg{\cdot}ha^{-1}$ at 1000 m to 250 $Mg{\cdot}ha^{-1}$ at 1300 m (Asner et al. 2008*a*), simultaneous to a reduction in average canopy height from 24 to 14 m (Fig. 3).

The lower portion of the transect begins above

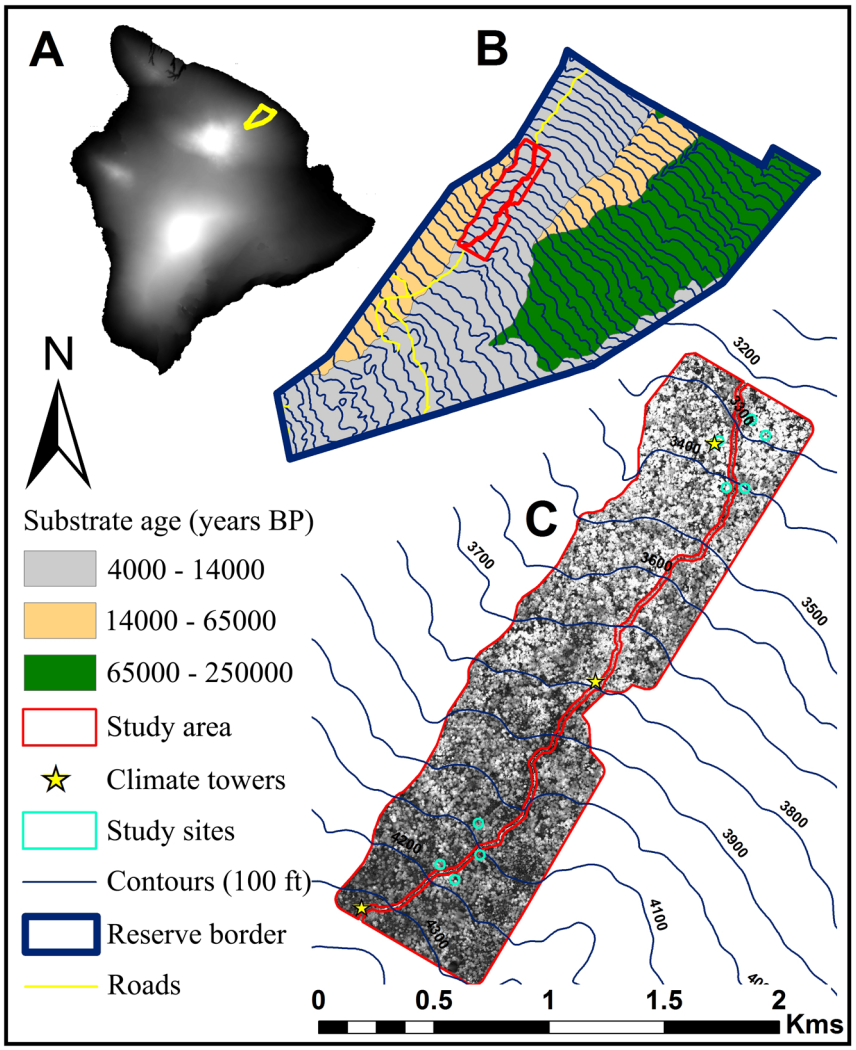

Fig. 2. Study area (C) located within the Hawaii Experimental Tropical Forest (B) in Laupahoehoe, Hawai'i (A). Inset C provides tree height at 1.25 × 1.25 m resolution, with heights ranging from 0 m (black) to 40 m (white).

a biological invasion front ending around 900 m dominated by *Psidium cattleianum* (Myrtaceae) and *Ficus rubiginosa* (Moraceae) and ends below an area of natural *M. polymorpha* dieback (Mueller-Dombois 1987). Understory plant composition is dominated by tree ferns (*Cibotium* sp.), and the small trees *Cheirodendron trigynum* ssp. *Trigynum* (Araliaceae), *Ilex anomala* (Aquifoliaceae), *Myrsine lessertiana* (Myrsinaceae) and *Coprosma rhynchocarpa* (Rubiaceae). The primary animal source of disturbance—constant throughout the study transect—consists of non-native feral pigs (*Sus scrofa*) which root the forest floor and propagate invasive species (Stone et al. 1992).

Study plots

Study plots were established at low (~1000 m) and high (~1300 m) elevations and positioned to encompass the range of forest structure found in the study transect. Six plots were located between 1000 and 1050 m and five between 1250 and 1300 m elevations. We established a 2 m by 30 m transect within each study plot ($N = 8$). Data were collected for each stem greater than 0.5 m in height and included elevation (1000 or 1300 m), species, native vs. non-native status, height (m), and diameter (cm; at breast height

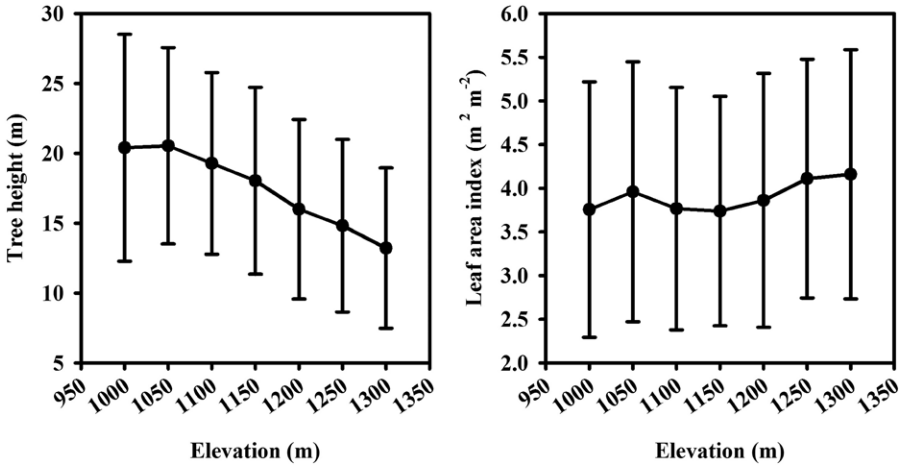

Fig. 3. Tree height (m) and leaf area index (LAI; m^2/m^2) for 50 m elevation classes. Data derived from airborne hyperspectral imagery (1.25 × 1.25 m resolution) with $N > 500{,}000$ pixels per elevation class.

when applicable, i.e., DBH). Volume (cm^3) was calculated as basal area (cm^2) multiplied by height (cm). Density (D = no. of individuals/1000 m^2), dominance (Do = $\sum$ volume of all individuals/1000 m^2) and frequency (F = number of transects containing the species) were calculated for each species. An importance value (IV) was calculated for each species using relative percent values (R) as compared to the median of all species, calculated as:

$$\mathrm{IV} = [RD \times 100] + [R\mathrm{Do} \times 100] + [RF \times 100] \quad (1)$$

modified from Busby et al. (2010) and Curtis and McIntosh (1951). Georeferenced marker stakes were established within each study plot using a differentially corrected geographic positioning system (GPS) unit (GS-50+, Leica Geosystems, St. Gallen, Switzerland) incorporating multiple-bounce filtering. Following 6 to 8 hours of 5-second interval GPS data collection per marker (N = 10) final post-differential correction horizontal (XY) and vertical (Z) uncertainty were 19 ± 13 and 33 ± 24 cm (mean ± SD), respectively.

Georeferencing

All interior forest measurements were georeferenced vertically and horizontally for integration with remote sensing data. The georeferencing procedure consisted of mounting a laser rangefinder with integrated inclinometer and 3D compass (Trupulse 360B, Laser Technology, Centennial, Colorado, USA) using filter mode and reflectors to avoid erroneous pulse returns on a tripod a known height (mh; cm) directly above a study plot marker stake. Position data returned from the Trupulse included the straight-line distance (sd; in meters), inclination (inc; in degrees) and azimuth (az; in degrees) from magnetic north. Prior to offset calculations, azimuth was adjusted to degrees from true north by adding a declination of 9.75° (www.ngdc.noaa.gov/geomagmodels/struts/calcIGRFWMM). Locations of offset locations were then calculated from the marker stake as:

$$\mathrm{hd} = \mathrm{sd} \times \cos(\mathrm{inc}) \quad (2)$$

$$x\ \mathrm{offset} = \mathrm{hd} \times \sin(\mathrm{az}) \quad (3)$$

$$y\ \mathrm{offset} = \mathrm{hd} \times \cos(\mathrm{az}) \quad (4)$$

$$z\mathrm{offset} = \mathrm{sd} \times \sin(\mathrm{inc}) + \mathrm{mh} \quad (5)$$

where hd = horizontal distance (in meters), and x, y and z offsets are in meters from the marker stake. An accuracy assessment of geolocation offsets showed single offsets were accurate to <30 cm in the vertical and horizontal dimensions over a wide range of distances (11–22 m), whereas double offsets, required in only a few instances when the marker stake had an obstructed view of the measurement location, were accurate to <64 cm vertically and horizontally.

Climate measurements

Both top-of-canopy (TOC) climate and interior forest microclimate measurements were collected. TOC measurements were acquired continuously by stations at 1052 (i.e., low), 1180 (i.e., mid), and 1353 (i.e., high) m elevation, evenly spaced along the transect. TOC sensors at low and high-elevations consisted of a total quantum sensor (SQ-110, Apogee Instruments, Logan, Utah, USA), temperature and relative humidity, a sonic anemometer and precipitation (WXT-510, Vaisala, Helsinki, Finland) downloaded to a datalogger (CR-200, Campbell Scientific, Logan, Utah, USA). The mid-elevation sensor array consisted of a direct/diffuse quantum sensor (BF3, Delta-T Devices, Cambridge, UK), a total quantum sensor (LI-190, LI-COR, Lincoln, Nebraska, USA), and temperature and relative humidity sensors (HMP45C-L20, Vaisala) downloaded to a datalogger (CR-3000, Campbell Scientific). Climate data collected every 15 seconds was averaged to a one-minute interval, with the exception of rainfall data that was the sum total each minute. Four mobile interior forest micro-climate stations were constructed, each consisting of a quantum sensor (SQ-110, Apogee Instruments), a temperature and relative humidity sensor (HOBO U23-002, Onset Computer, Bourne, Massachusetts, USA) and a cup anemometer (200-WS-01, Novalynx, Auburn, California, USA). PAR measurements, from the quantum sensors, and wind speed data were downloaded to a datalogger (CR-10x, Campbell Scientific) while temperature and relative humidity data were internally logged. Microclimate data were logged every 15 seconds and averaged to one-minute intervals. In addition, PAR data were logged every three seconds for the initial five minutes of each hour.

TOC PAR sensors were intercalibrated using known clear sky days to the mid-elevation quantum sensor, which was recalibrated annually, and calibration drift was removed using a clear sky PAR model coded in the R language (R Development Core Team 2013) and modified from equations provided by Apogee Inc. and as developed by the American Society of Civil Engineers (2005) (see Supplement for code). This model uses day of year, time of day, latitude, longitude, elevation, air temperature, and relative humidity as input variables and has been validated to estimate clear sky PAR within 3% at solar noon. Interior forest quantum sensors were intercalibrated weekly in an open field for two hours with data logged every 15 seconds averaged to one-minute intervals and returned for recalibration several times a year.

Leaf traits

Leaf trait measurements included light, CO_2 and induction gas exchange response curves, foliar mass per area, elemental C and N percentage, and $\delta^{13}C$ and $\delta^{15}N$ stable isotopes. Foliar gas exchange measurements were acquired using a LI-6400 portable infrared gas analyzer (LI-COR) on the dominant species identified by the species importance values. Single and double rope tree climbing techniques were used to collect in situ foliar gas exchange above 2.5 m in height, while tripods were used below that height. Additional data collected at each measurement location were: (1) species, (2) time and date, (3) DBH, (4) height of measurement, and (5) total height of plant. Photographs were collected for identification by botanists at the University of Hawaii at Hilo in cases where the species was not identified in the field. Gas exchange measurements were acquired at ambient leaf temperature, between 23° and 27°C, on mature leaves with relative humidity maintained between 65% and 75% and following a minimum 30-minute LI-COR 6400 stabilization period. Most measurements were conducted with the cuvette leaf area at capacity (6 cm^2); however, when leaves smaller than 6 cm^2 were used, leaf area was measured in the field and gas exchange measurements were adjusted accordingly. Each of the three response curves were collected on separate leaves located immediately adjacent to each other and having similar characteristics. Curves were measured between the hours of 09:00 and 16:00 at a flow rate of 400 $mol{\cdot}air{\cdot}s^{-1}$.

Light response curves were collected at a constant reference chamber CO_2 concentration ($\mu mol{\cdot}CO_2{\cdot}mol^{-1}$ air) of 400 and by increasing the photosynthetic photon flux density (PPFD or Q; $\mu mol{\cdot}m^{-2}{\cdot}s^{-1}$), i.e., encompassing the 400–700 nm wavebands, stepwise from zero through saturating PPFD using the following increments: 0, 20, 40, 60, 80, 100, 130, 160, 200, 250, 300, 400, 800, and 1600. Measurements at each PPFD were logged when gas exchange was stable as indicat-

ed by: (1) visually stable intracellular CO_2 concentration (C_i; μmol·CO_2·mol·air^{-1}) and net CO_2 assimilation rates (A; μmol·CO_2·m^{-2}·s^{-1}) values, (2) a total coefficient of variation (CV) percentage (calculated as the sum of CO_2 and H_2O CV percent) of less than 0.1% and (3) following a min-max wait time of 3–10 minutes, respectively. CO_2 response curves, CO_2 assimilation rates versus the intracellular CO_2 concentration (AC_i), were collected at saturating PPFD + 200 (μmol·m^{-2}·s^{-1}) identified by the light response curve. Following a five-minute stabilization period at a reference chamber CO_2 concentration (μmol·CO_2·mol^{-1}·air) of 100, CO_2 concentration was increased stepwise through the following increments: 100, 300, 600, 900, 1200, and 1500. Measurements were logged at each increment using the same criteria as for light response curves, but with min-max time adjusted to 3–5 minutes, respectively. Induction response curves were collected following a five-minute stabilization period at a PPFD of 20. During the last 30 seconds of stabilization, measurements were logged every two seconds, following which PPFD was increased directly to 1300, and logging continued every two seconds for 3–5 minutes. Prior to analysis measurements from the light and CO_2 response curves were normalized for differences in leaf temperature to A at 25°C through a custom version of the SiB2 photosynthesis model (Sellers et al. 1996) coded in IDL (Interactive Data Language, ITTVIS, Boulder, Colorado, USA, 2000–2010) and provided by Joseph Berry (Department of Global Ecology, Carnegie Institution for Science, Stanford, California, USA, *personal communication*).

Normalized light (AQ) and CO_2 (AC_i) response curves were fit through non-linear parameterization using the LI-COR Photosynthesis software (Version 1.0, LI-COR) available online: ftp://ftp.licor.com/perm/env/LI-6400/Software/analysis_software/Photosynthesis.exe [accessed 06/03/2011]. AQ curves were fit to:

$$A = \frac{\varnothing \times Q}{[1 + \left(\frac{\varnothing \times Q}{A_{max}}\right)^{p}]^{1/p}} + A_0 \quad (6)$$

where A (i.e., A_{area}) is the net CO_2 assimilation (μmol·CO_2·m^{-2}·s^{-1}) per area, A_{max} is the maximum rate of A (the asymptote), $\varnothing$ is the apparent quantum efficiency (i.e., the initial slope of the fit hyperbola), p is the curve convexity parameter, A_0 is the dark respiration rate (μmol·CO_2·m^{-2}·s^{-1}) and Q is the incident PPFD (μmol·m^{-2}·s^{-1}). In addition, the light compensation point and light saturation estimate (μmol·m^{-2}·s^{-1}) were calculated as Q value at which A = zero and the linear intersection of $\varnothing$ and A_0 with A_{max}, respectively.

AC_i curves were fit to a biochemical model of photosynthesis developed by Farquhar et al. (1980) and updated to account for triose-phosphate limitation (TPU) as described in Long and Bernacchi (2003), where net CO_2 assimilation (A) per area, dependent solely on mesophyll processes, is determined by the minimum of three potential limiters: Rubisco activity (V_{cmax}; W_c), RuBP regeneration (J_{max}; W_j) or the regeneration and utilization of inorganic triose-phosphate (V_{TPU}; W_p). Limitation typically shifts from W_c to W_j to W_p with increasing C_i, calculated by:

$$W_c = \frac{V_c max \times C_i}{[C_i + K_c(1 + {}^{O}/_{K_o})]} \quad (7)$$

where V_{cmax} is the maximum rate of carboxylation by Rubisco (μmol·CO_2·m^{-2}·s^{-1}), K_c and c are the Michaelis-Menten constants of Rubisco for CO_2 and O_2, respectively, and O is the stroma O_2 concentration (Pa).

$$W_j = \frac{J \times C_i}{4.5 \times C_i + 10.5 \times \Gamma} \quad (8)$$

where $\Gamma = 0.5 \times O/\tau$; τ is the specificity factor for Rubisco, and J, the whole chain electron transport rate, is:

$$J = \frac{Q_2 + J_{max} - \sqrt{(Q_2 + J_{max})^2 - 4\theta_{PSII} Q_2 J_{max}}}{2\theta_{PSII}} \quad (9)$$

with θ_{PSII} = curvature factor, Q_2 = incident quanta available to PSII, and:

$$Q_2 = Q \underset{1}{\propto} \varnothing_{PSIImax} \beta \quad (10)$$

where $\propto_1$ = leaf absorptance, $\varnothing_{PSII,max}$ = max quantum yield of PSII, and β = fraction absorbed light accessible by PSII.

$$W_p = \frac{3 \times TPU}{\left(1 - \frac{\Gamma}{C_i}\right)} \quad (11)$$

where V_o is the rate of oxygenation of Rubisco and TPU is rate of triose phosphate utilization

($\mu mol \cdot CO_2 \cdot m^{-2} \cdot s^{-1}$). The determination of A at C_i (x) is:

$$A = \left(1 - \frac{\Gamma}{C_i}\right) \times \min(W_c, W_j, W_p) - R_{day} \quad (12)$$

where R_{day} represents the CO_2 released through non-photorespiration processes ($\mu mol \cdot CO_2 \cdot m^{-2} \cdot s^{-1}$).

Induction response data were analyzed through non-linear parameterization of a two parameter modified rectangular hyperbola model in JMP software (Version 7; SAS Institute, Cary, North Carolina, 1989–2007) developed for induction response analysis (Hunt et al. 1991, Poorter and Oberbauer 1993). The model is defined as:

$$A_t = \frac{A_{max} \times k_i \times t}{A_{max} + k_i \times t} \quad (13)$$

where A_t is assimilation at time t (seconds), k_i is the induction curve convexity, t is seconds post-PPFD increase and A_{max} is net CO_2 assimilation per unit area. Using the output A_{max} value, the input data were then converted to induction state, redefining A as percentage of A_{max} at time t (seconds) post-induction, and the equation was then reparameterized using an A_{max} equal to 100% to obtain k_{is}, a value comparable across leaves varying in A_{max}. Output results for statistical analysis were the estimated A_{max}, k_i, k_{is}, and time (seconds) to 50% induction state (IS50%) calculated as:

$$t = -\frac{IS \times A_{max}}{(IS - 100)k_i} \quad (14)$$

where t is time post induction in seconds, IS equals the induction state (%), and A_{max} and k_i are as defined above.

All leaves on which gas exchange measurements were conducted were collected and scanned at 600 dpi (x9575, Lexmark International, Lexington, Kentucky, USA) for leaf area calculation in Photoshop (CS, Adobe Systems, San Jose, California, USA) within 12 hours. Leaves were then oven dried at 55°C for 48–56 hours, weighed (0.01 mg; Mettler Toledo AG245), and ground to a fine powder using a Wiley Mill (Thomas Scientific, Swedesboro, New Jersey, USA) fitted with a 40-mesh screen. Samples were analyzed for C and N concentration, and $\delta^{13}C$ and $\delta^{15}N$, using a Vario Microcube elemental analyzer (Elementar Analysensysteme, Hanau, Germany) coupled to an isotope ratio mass spectrometer (Isoprime, Manchester, UK) operating in continuous flow mode at the Stable Isotope Laboratory at Tulane University. Samples were normalized to international isotope scales by bracketing with USGS-40 and USGS-41 glutamic acid standards (calibrated to the international VPDB ($\delta^{13}C$) and AIR ($\delta^{15}N$) scales) and repeated analysis of sorghum flour was used to assess instrumental drift during runs as well as differences between runs. Stable isotope data are expressed using "delta" notation (Ometto et al. 2006).

Additional variables were defined as follows: specific leaf area (SLA) is the projected leaf area per unit leaf dry mass (cm^2/g) (Evans and Poorter 2001, Martin and Asner 2009, Liu et al. 2010), leaf mass per area (LMA; g/m^2) (Cordell et al. 1998), N_{area} is nitrogen content per area (g/m^2) (Ellsworth and Reich 1993, Dang et al. 1997, Cordell et al. 1998), photosynthetic nitrogen use efficiency (PNUE) is the ratio of A_{max} to N_{area} ($\mu mol \cdot CO_2 \cdot s^{-1} \cdot mol^{-1}$ N) (Cordell et al. 1998, Funk and Vitousek 2007), water use efficiency (WUE) is the ratio of A_{area} to transpiration rate ($\mu mol \cdot CO_2$ per mmol H_2O) under saturating PAR (Funk and Vitousek 2007), and A_{mass} is the ratio of A_{max} to unit leaf dry mass ($nmol \cdot CO_2 \cdot g^{-1} \cdot s^{-1}$) (Ellsworth and Reich 1992). We also calculated the ratio of IS50%/A_{max}, to understand optimization of induction response time, which we included in the Akaike Information Criteria (AIC) and best subsets regression analyses described in *Data integration*, below.

Airborne remote sensing

The study transect was imaged by the Carnegie Airborne Observatory (CAO) Alpha sensor system in January 2008 at a height of 500 ± 50 m. The CAO-Alpha integrated a high-fidelity hyperspectral imager (HiFIS) having 72 bands distributed from 368 to 1040 nm, a waveform LiDAR (wLIDAR) scanner operating at 1064 nm and 100 kHz and a Global Positioning System-Inertial Measurement Unit (GPS-IMU). An automated processing stream incorporated ortho-georectification and atmospheric correction for a final spatial accuracy of <15 cm in the vertical or horizontal dimension (Asner et al. 2007). HiFIS data had a final spatial resolution of 1.25 m while wLiDAR data were collected at 0.56 m. wLiDAR

pre-processing included noise reduction, deconvolution, waveform registration and angular rectification (Wu et al. 2011). wLiDAR point clouds were processed to proportional data by summing points within 0.56 × 0.56 × 0.15 m (XYZ) voxels, and dividing each voxel's value by the summed total points in each 0.56 × 0.56 m vertical profile throughout the study transect. Ground and tree crown topography maps were generated through analysis of point cloud data. Solar azimuth at time of data collection was calculated in IDL using solar geometry and tree crown topography.

LAI (m^2 leaf area/m^2 ground area) was calculated using paired LAI-2000 (LI-COR) units in remote mode for 49 locations randomly distributed throughout the study transect at a height of 155 cm. We calculated a map of the top-of-canopy cosine angle to the sun using the tree (primarily *M. polymorpha*) canopy topography maps and per-pixel acquisition time. HiFIS data were resampled to 0.56 × 0.56 m from 1.25 × 1.25 m spatial resolution to be directly comparable with the wLiDAR data using the nearest neighbor method. The modified red edge normalized difference vegetation index (mNDVI; see Gitelson and Merzlyak 1996 and Gamon and Surfus 1999):

$$\mathrm{mNDVI}_{705} = \frac{\rho_{750} - \rho_{705}}{\rho_{750} + \rho_{705} - 2\rho_{445}} \qquad (15)$$

was applied to the image and we then removed the effect of shade through a linear regression between mNDVI extracted for a 2 m radius surrounding each LAI field location and the cosine value ($P < 0.0001$; $R^2 = 0.5367$), then calculated LAI as the linear relationship between field calculated LAI values and the difference between the cosine predicted mNDVI value and that calculated from the image. The final relationship was highly significant ($P < 0.01$; $R^2 = 0.3401$; $N = 49$) and was applied to the entire HiFIS image to derive a detailed LAI map of the study area.

Leaf area density (LAD), defined as m^2 of leaf area per m^3 of volume, was calculated throughout the study area using the proportional data derived from the corrected wLiDAR points. Three-dimensional maps of LAD were calculated by converting two-dimensional LAI values from m^2 to pixel scale (0.56 × 0.56 m = 0.3136 m^2) and distributing the leaf area across the vertical profile according to the proportion values obtained from the wLiDAR proportion maps at a vertical resolution of 0.15 m, as below:

$$\mathrm{LAD}(x) = \mathrm{LAI} \times 0.3136 \times \mathrm{pwf}(x) \qquad (16)$$

where LAD = leaf area (m^2) within the vertical profile (0.56 × 0.56 m) at height x to $x + 0.15$ m, LAI = leaf area index (m^2 leaf/m^2 ground area), and pwf = proportion waveform LiDAR points occurring at x.

The wLiDAR correction process was validated for this study site using field leaf area density profiles ($N = 13$) ranging from 10 to 24 m in height with horizontal and vertical resolution of a 0.2463 m^2 and 0.5 m, respectively. Field LAD profiles were collected across diverse forest structure types by establishing and rappelling off horizontal Tyrolean rope traverses between tree canopies, collecting all leaves and measuring their collection height using an ultrasonic range finder (SONIN, Charlotte, North Carolina, USA) with a sonic target to reduce erroneous returns. Leaves were stored in zip lock bags with moist paper towels until leaf area (cm^2) was calculated within 24 hours using a LI-3100 (LI-COR). A significant linear relationship was shown between the cumulative percentage of leaf area identified rebinned to comparable vertical (0.5 m) and horizontal (pixel area of 0.3136 m^2) resolution ($P < 0.0001$; $R^2 = 0.4960$; $N = 404$), and no significant difference in LAD values was identified in a matched pairs analysis ($P > |t| = 0.1253$; $N = 404$). Virtual forests were then generated through integration of the surface elevation and 3D LAD (cm^2) data, which were used in the subsequent modeling analyses.

Interior forest microclimate modeling

Interior forest climate data were compared to interpolated TOC climate data at each study plot center point. TOC values were derived from the weighted average—based on elevation—of the most proximate pair of TOC sensors. For example, for a position located between the mid and high TOC towers the interpolated TOC values would be:

$$p = \frac{(\mathrm{TOC}_{\mathrm{interior}} - \mathrm{TOC}_{\mathrm{mid}})}{(\mathrm{TOC}_{\mathrm{high}} - \mathrm{TOC}_{\mathrm{mid}})} \qquad (17)$$

$$\mathrm{TOC}_{\mathrm{interp}}=(\mathrm{TOC}_{\mathrm{high}}\times p)+\Big(\mathrm{TOC}_{\mathrm{mid}}\times(1-p)\Big). \quad (18)$$

Interpolated total PAR values were proportioned according to diffuse and direct PAR measured at the mid elevation tower which was the only location with a BF3 direct vs. diffuse sensor installed. Separate direct and diffuse PAR models were developed. Direct PAR utilized solar azimuth and elevation calculated through interpolation of National Aeronautics and Space Administration (NASA) Jet Propulsion Laboratory (JPL) planetary ephemeris (DE405; http://ssd.jpl.nasa.gov) using IDL code modified from that provided by Craig Markwardt (http://cow.physics.wisc.edu/~craigm).

The direct PAR model calculated the distribution of leaf area density at 0.25 m increments from zero to 100 m distance from the sensor directly towards the sun position, which was calculated at one-minute intervals. LAD was then adjusted according to its distance from the sensor using the following equation:

$$\mathrm{DirSF}=\sum\Big(-k\times\mathrm{sd}\times\mathrm{LAD}(x)\Big) \quad (19)$$

where DirSF is the direct structure factor, k is the extinction parameter set to 0.025, sd is the straight-line Euclidean distance from the sensor (x), and LAD is the leaf area density (cm^2) encountered at distance (x). DirSF calculation was limited to the daytime, defined as solar elevations $\geq$25°. The diffuse PAR model used the same approach for each location to calculate the diffuse structure factor (DifSF) but averaged DirSF values from 36 combinations of azimuth and elevation (>22.5°) equally distributed across a hemisphere above the sensor.

Total interior forest PAR was modeled at one-hour intervals using the averaged PAR and structure data. Interior PAR was calculated:

$$\mathrm{tPAR}_{\mathrm{int}(t)}=a+b\times\mathrm{tPAR}_{\mathrm{TOC}}(t)-c\times\mathrm{tDirSF}+d\times\mathrm{DifSF} \quad (20)$$

$$\mathrm{PAR}_{\mathrm{int(t)}}=1.09\times\Big(\Big(\mathrm{tPAR}_{\mathrm{int(t)}}\times0.24+1\Big)\wedge(1/0.24)\Big). \quad (21)$$

The constants a–d equal: 2.3638, 0.3633, 0.0304 and 3.792E-04, respectively. $\mathrm{tPAR}_{\mathrm{toc}}$ and tDirSF represent power transformed (t; i.e., $(U\wedge\lambda)-1/\lambda$) versions of the raw variables conducted to normalize residual distributions using lambda values of 0.28 and 0.44, respectively. Parameterization was conducted in JMP on a randomly selected 50% of the available interior forest data during daylight hours. The remaining data were used to validate the model. Both the parameterization model ($P<0.0001$, $R^2=0.6566$, $N=355$) and validation ($P<0.0001$, $R^2=0.6622$, $N=371$) were highly significant.

Average air temperature was predicted at each sensor location using the environmental lapse rate calculated at 30-minute increments as follows:

$$\mathrm{Temp}_{\mathrm{pred}(t)}=(\mathrm{INT}_{\mathrm{elev}}-\mathrm{MID}_{\mathrm{elev}})\times\mathrm{MLR}(t)+\mathrm{MID}_{\mathrm{temp}}(t) \quad (22)$$

where $\mathrm{Temp}_{\mathrm{pred}}$ is the predicted air temperature (°C) at time t and $\mathrm{INT}_{\mathrm{elev}}$ is the elevation at the interior forest sensor. $\mathrm{MID}_{\mathrm{elev}}$ and $\mathrm{MID}_{\mathrm{temp}}$ is the elevation and air temperature at the mid elevation climate tower, and MLR is the mean environmental lapse rate calculated among the high, mid and low elevation climate towers. This relationship was highly significant ($P<0.0001$, $R^2=0.7975$, $N=4713$).

The final forest interior air temperature model compared the measured versus the predicated air temperatures as influenced by DirSF and DifSF as:

$$\left(\frac{\mathrm{Temp}_{\mathrm{meas}}}{\mathrm{Temp}_{\mathrm{pred}}}\right)=a-b\times\sqrt{\mathrm{DirSF}}+c\times\mathrm{DifSF}. \quad (23)$$

The constants a–c equal: 1.014, 6.1687E-04, and 4.984E-06, respectively. The sample size was reduced as DirSF was calculated for daytime hours only. The model was parameterized and validated as described for PAR above and was highly significant ($P<0.0001$, $R^2=0.8914$, $N=1529$).

Data integration

An overview of the data integration approach is illustrated in Fig. 1. For each location where ecophysiological data were collected, 4400 minutes of daytime climate data were randomly selected between December 17, 2010 and June 1, 2011, averaged to half hour intervals, and the following variables were calculated using the

field data collection, climate models and remote sensing data: (1) ground elevation (m), (2) canopy, plant and leaf height above forest floor (m), (3) DBH (cm), (4) mean and standard deviation of modeled available PPFD, and (5) modeled average air temperature (°C). Highly correlated variable groups were identified using Pearson correlation analysis (>0.7), resulting in the final selection of the leaf trait predictor variables: (1) leaf height, (2) PPFD mean and (3) SD, and (4) mean air temperature. Ground elevation, although highly correlated with mean air temperature, was included as well to account for potential unquantified variation in climate and forest dynamics along the elevation gradient.

Predictor variables were transformed, when appropriate, to create a normal distribution, and the importance of all variables on each ecophysiological variable was assessed using: (1) community scale; best subsets multiple regressions with the most significant combinations of predictor variables identified using the adjusted R^2 value, and (2) for the dominant canopy and understory species—*M. polymorpha* (Ohia) and *C. glaucum*, respectively—and the entire species community, linear regressions between selected ecophysiological variables and leaf height, PPFD mean, and air temperature mean. Separate general linear models were fit to understand differences due to the following classifications: (1) species, (2) life-form, (3) exotic vs. native, (4) height strata, (5) canopy position, and (6) *M. polymorpha* or other. Life forms were defined as herb, fern, liana, shrub, tree fern, understory tree or canopy tree. Height strata were defined as ground, mid or upper. Canopy positions were defined as understory or canopy. Models were compared using AIC values (Mazerolle 2006, Mutua 1994) and weight (Anderson 2008), which adjusts for differences in parameter size, using identical data sets. AIC provides a method to compare relative model goodness of fit for a specific foliar variable, with models $\Delta_i > 10$ above the minimum AIC having little support (Burnham and Anderson 2004). For our analysis, we kept the two best models and discarded those having AIC values $\Delta_i > 20$.

We sought to identify groups having similar ecophysiological characteristics using two approaches. We used principal components analysis (PCA; Reich et al. 1999) to assess if general trends in ecophysiological variables ($N = 22$) existed. We then identified significant correlations between PCA axes and box-cox transformed, for increase normality, PPFD and air temperature. We clustered the foliar dataset into three groups through *K*-means analysis using the first three PCA axes and compared ecophysiological, structural, and climatic variables among these groups using one-way ANOVAs and Pearson tests.

Results

Plant diversity and structure

Top-of-canopy (TOC) height declined from 20.4 ± 8.1 m at 1000–1049 m elevation to 13.2 ± 5.7 m at 1300–1349 m elevation (Fig. 3). LAI remained constant across the study area (3.9 ± 1.4 m^2/m^2). A total of 24 species were identified in the plant diversity transects (Table 1). Importance values ranged widely, with *M. polymorpha, C. glaucum* and *C. trigynum* identified as the three most important species (Table 2). The canopy was comprised almost exclusively of *M. polymorpha,* although its seedlings and saplings also existed in more open understory environments, with the next strata comprised mostly of *C. trigynum*, *C. rhynocarpa*, and *I. anomala*. A final strata occurring at 3–5 m height consisted almost entirely of *C. glaucum*. Species growing below 2 m included an abundance of the exotic species *H. gardnerianumi* and occasional *P. cattleianum* individuals. Open wet areas at low elevations were dominated by the exotic species *P. punctata* (Smartweed) below 1 m height, with shrubs including young *M. polymorpha* and the exotic species *C. hirta*.

Microclimate

Table 3 summarizes mean TOC climatic conditions recorded at the low, mid and high elevation towers between December 17, 2010 and May 16, 2011. Seasonal dynamics of PPFD and air temperature are provided in Fig. 4 and diurnal dynamics are provided in Fig. 5. Measured mean air temperature dropped from 15.93° to 14.13°C from the low to high elevation tower respectively. The low elevation tower received 58% more rainfall than the high elevation tower. Total daytime PAR was nearly equal among the low, mid and high elevation locations with the mean

Table 1. Plant species occurring within diversity transects.

Family	Genus	Species	Common name	Status	Life-form
Myrtaceae	*Metrosideros*	*polymorpha*	Ohia	Native	Canopy tree
Cibotiaceae	*Cibotium*	*glaucum*	Hapu'u-pulu	Native	Tree fern
Araliaceae	*Cheirodendron*	*trigynum*	Olapa	Native	Understory tree
Polygonaceae	*Persicaria*	*punctata*	Water smartweed	Exotic	Herb
Rubiaceae	*Coprosma*	*rhyncocarpa*	Pilo	Native	Understory tree
Aquifoliaceae	*Ilex*	*anomala*	Hawai'i holly	Native	Understory tree
Zingiberaceae	*Hedychium*	*gardnerianum*	Kahili ginger	Exotic	Herb
Dryopteridaceae	*Dryopteris*	*wallichiana*	Laukahi	Native	Fern
Aspleniaceae	*Asplenium*	*contiguum*	Asplenium	Native	Fern
Pandanaceae	*Freycinetia*	*arborea*	Ie'ie	Native	Liana
Rosaceae	*Rubus*	*hawaiensis*	Akala	Native	Shrub
Celastraceae	*Perrottetia*	*sandwicensis*	Olomea	Native	Understory tree
Dryopteridaceae	*Dryopteris*	*glabra*	Kilau	Native	Fern
Cyatheaceae	*Cyathea*	*cooperi*	Australian tree fern	Exotic	Tree fern
Myrtaceae	*Psidium*	*cattleianum*	Strawberry guava	Exotic	Understory tree
Rubiaceae	*Psychotria*	*hawaiiensis*	Kopiko	Native	Understory tree
Athyriaceae	*Athyrium*	*microphyllum*	Akolea	Native	Fern
Melastomataceae	*Clidemia*	*hirta*	Koster's curse	Exotic	Shrub
Rutaceae	*Melicope*	*clusiifolia*	Alani	Native	Understory tree
Liliaceae	*Astelia*	*menziesiana*	Painiu	Native	Herb
Ericaceae	*Vaccinium*	*calycinum*	Ohelo	Native	Shrub
Rubiaceae	*Hedyotis*	*hillebrandii*	Manono	Native	Understory tree
Apocynaceae	*Alyxia*	*olviformis*	Maile	Native	Liana
Campanulaceae	*Clermontia*	*parviflora*	Haha	Native	Shrub

Table 2. Plant density (no. individuals/1000 m^2), volume (basal area $\times$ height cm^3), frequency (% transects occurring) of species found within diversity transects. Species are ranked by their importance value (IV). Sampled (cluster) = whether foliar samples were collected and to which cluster the species was assigned. Species taxonomic information is provided in Table 1. Height and DBH values are expressed as mean $\pm$ SD.

Common name	Density	Vol. (cm^3)	Freq. (%)	Height (m)	DBH (cm)	IV	Rank	Cluster
Ohia	85	1108099715	100	11.6 ± 8.5	63.7 ± 66.1	3522722	1	1
Hapu'u-pulu	250	20514819	100	2.8 ± 2.0	14.3 ± 7.8	66115	2	1
Olapa	137	4620076	100	4.5 ± 3.4	5.0 ± 5.0	15285	3	1
Water smartweed	4533	7120	37.5	0.5 ± 0.0	0.2 ± 0.0	12379	4	
Pilo	91	1382914	100	3.8 ± 2.8	3.7 ± 3.5	4871	5	3
Hawai'i holly	50	894898	75	3.1 ± 2.4	4.1 ± 5.9	3151	6	1
Kahili ginger	506	244571	50	1.5 ± 0.3	2.0 ± 0.1	2262	7	2
Laukahi	98	398655	75	0.9 ± 0.3	7.2 ± 2.0	1703	8	3
Asplenium	59	179112	50	0.8 ± 0.2	6.8 ± 1.3	842	9	
Ie'ie	148	12729	37.5	0.8 ± 0.4	1.0 ± 0.3	526	10	3
Akala	67	9096	62.5	1.0 ± 0.4	0.9 ± 1.0	354	11	2, 3
Olomea	11	49204	50	3.4 ± 2.0	2.8 ± 2.1	300	12	2, 3
Kilau	33	30152	50	0.8 ± 0.3	2.5 ± 2.7	298	13	
Australian tree fern	4	62924	12.5	1.2 ± 0.5	12.5 ± 0.7	240	14	
Strawberry guava	30	11007	37.5	1.7 ± 1.1	1.03 ± 0.6	203	15	3
Kopiko	11	27416	37.5	2.8 ± 1.9	2.3 ± 1.6	202	16	
Akolea	13	13534	50	0.8 ± 0.3	3.8 ± 1.3	193	17	
Koster's curse	41	13686	12.5	1.2 ± 0.6	1.3 ± 0.9	184	18	2
Alani	9	32768	12.5	4.3 ± 1.5	3.0 ± 1.4	156	19	
Painiu	2	33450	12.5	1.0 ± 0.0	14.0	141	20	
Ohelo	28	664	12.5	1.2 ± 0.4	0.4 ± 0.2	107	21	
Manono	4	5431	25	2.0 ± 2.1	1.9 ± 1.6	86	22	3
Maile	13	41	12.5	1.0 ± 0.0	0.2 ± 0.0	64	23	
Haha	2	576	12.5	1.5 ± 0.0	1.5	36	24	

Table 3. Daytime (sun elevation > 25°C; mean ± SD) climatic conditions at top of canopy tower low, mid, and high locations between December 17, 2010 and June 19, 2011. Rainfall is the total over this period.

Climate variable	Low (1052 m)	Mid (1180 m)	High (1353 m)
Air temperature (°C)	17.5 ± 2.0	16.9 ± 2.0	16.2 ± 2.2
Relative humidity (%)	79.3 ± 11.3	85.4 ± 13.5	77.2 ± 12.1
Windspeed (m/s)	2.5 ± 1.8	3.0 ± 1.3	2.1 ± 1.3
Wind direction (degrees true north)	258 ± 43	280 ± 66	252 ± 96
Direct PPFD (%)		34 ± 35	
Diffuse PPFD (%)		66 ± 35	
PPFD ($\mu mol \cdot m^{-2} \cdot s^{-1}$)	932 ± 572	909 ± 556	937 ± 559
Rainfall (mm total)	684.4		399.8

Note: PPFD = photosynthetic photon flux density.

diffuse percentage equaling 66% of daily PAR.

Leaf trait variation

Foliar C:N was highly correlated with SLA. A_{max} was significantly correlated with foliar %N and all CO_2 response variables, but not with LMA. Day respiration, however, was correlated with LMA (Table A1). General linear model results of categorical variables are presented in Table 4 and Table 5, with the most significant classifications being species (22/22), life form (18/22), and height strata (6/22). Elevation class was the most significant predictor of foliar $\delta^{15}N$ values. Both species and height strata were the most significant predictors of the light compensation point. Exotic versus native species, respectively, had significantly ($\alpha = 0.05$) greater foliar N (2.0 ± 0.8 vs. 1.4 ± 0.50), $\delta^{15}N$ (−0.75 ± 1.8 vs. −2.7 ± 1.8), IS50% (29.6 ± 16.8 vs. 14.5 ± 12.9) and A_{max} (6.8 ± 5.0 vs. 3.6 ± 1.8), but significantly lower day respiration (−0.34 ± 0.28 vs. −0.52 ± 0.24). In addition, V_{cmax} (19.3 ± 14.0 vs. 12.0 ± 6.6), J_{max} (14.7 ± 10.5 vs. 9.4 ± 5.8), and TPU (3.4 ± 2.5 vs. 2.1 ± 1.1) were significantly higher for exotic as compared to native species.

The best subsets multiple regression analysis revealed strong climatic and structural determinants of foliar ecophysiology (Tables 6 and 7). Most leaf traits were correlated with leaf height (20 of 24), followed by modeled mean PPFD (14 of 24), elevation (7 of 23), and modeled mean air temperature (7 of 24). Of all leaf traits, leaf height was most significantly correlated with foliar C (positive; adjusted $R^2 = 0.40$), followed by SLA (negative; adjusted $R^2 = 0.35$) and IS50% (negative; adjusted $R^2 = 0.36$). A_{max}, and associated %N, were strongly positively correlated with modeled mean PPFD, and foliar C:N was negatively correlated with modeled mean PPFD. While $\delta^{15}N$ was significantly positively correlated with modeled mean air temperature (adjusted $R^2 = 0.28$), $\delta^{13}C$ was not correlated with any structural or climatic variables. Rates of respiration increased with modeled air temperature but decreased with increasing leaf height.

Linear regressions between leaf traits and the predictor variables defined in Table 8 were calculated for *M. polymorpha* and *C. glaucum* (Table 8A, B), the overstory and understory species having the greatest importance values (Table 2), as well as across the entire community (Table 8C). Significant positive relationships existed between modeled mean PPFD and A_{max} across the community (adjusted $R^2 = 0.26$), and at the species scale for *M. polymorpha* (adjusted $R^2 = 0.13$) and *C. glaucum* (adjusted $R^2 = 0.40$). Light saturation was strongly correlated with modeled air temperature for *C. glaucum*. The dynamic response time (IS50%) of *C. glaucum* increased in higher modeled light environments, while that of *M. polymorpha* did not. Although increases in foliar C:N were shown at the community level (adjusted $R^2 = 0.18$), no such relationships existed within the individual species.

Leaf trait clusters

Principal components 1–3 encompassed 33.7%, 17.4%, and 10.6%, respectively, for a cumulative total of 62.6% of the variation (Table 9). Linear regression analysis revealed PCA axis one to have a significant positive correlation with modeled mean PPFD [$F = 38.6$ ($P < 0.0001$), adjusted $R^2 = 0.39$, $P \leq 0.0001$, df = 77], while PCA axis two and axis three did not have significant correlations with modeled mean PPFD [$F = 2.5$ ($P = 0.12$) and 3.6 ($P = 0.06$),

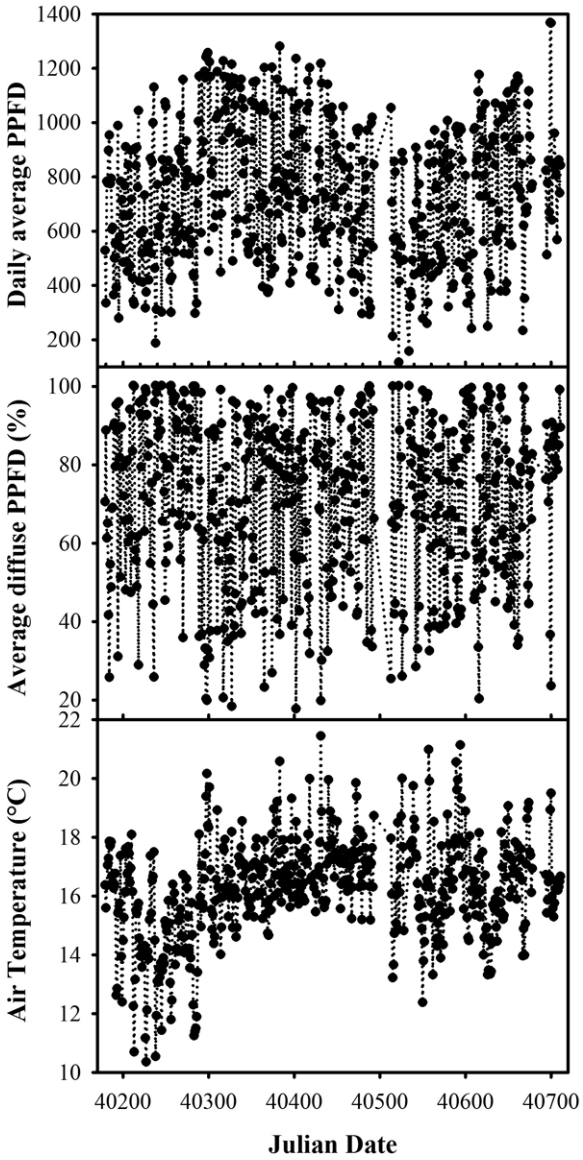

Fig. 4. Measured daily average daytime (solar elevation > 25°) photosynthetic photon flux density (PPFD; μmol·m^{-2}·s^{-1}), diffuse PPFD (%), and air temperature (°C) at the mid elevation top-of-canopy (TOC) climate tower. Julian dates extend from January 1, 2010 (40179 JD) through June 17, 2011 (40711 JD).

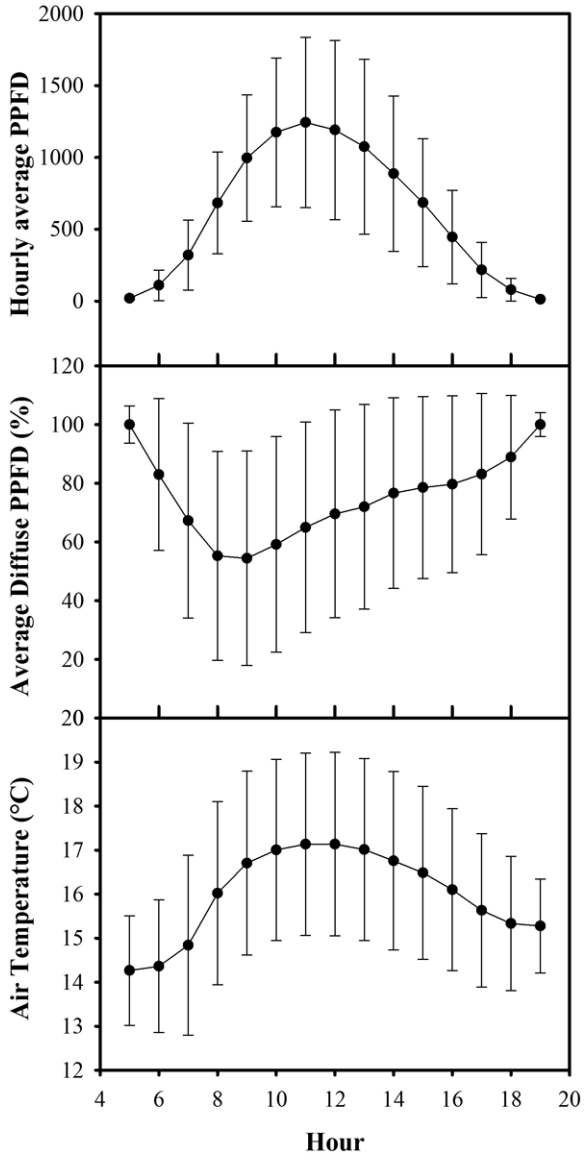

Fig. 5. Measured hourly mean daytime (solar elevation > 25°) photosynthetic photon flux density (PPFD; μmol·m^{-2}·s^{-1}), diffuse PPFD (%), and air temperature (°C) at mid elevation top-of-canopy climate tower.

respectively]. Multiple regression analysis using modeled mean PPFD and modeled mean air temperature as predictors and each individual PCA axis as the response revealed PCA axis one to have a significant positive relationship with modeled mean PPFD but not with modeled mean air temperature [model adjusted $R^2 = 0.35$, $P < 0.0001$; MM-PPFD and MM-air temperature $F = 22.2$ ($P < 0.0001$) and 0.04 ($P = 0.85$), respectively] while PCA axis two had a significant positive relationship with air temperature, but not PPFD [model adjusted $R^2 = 0.17$, $P = 0.0003$; MM-PPFD and MM-air temperature $F =$

Table 4. General linear model results for leaf traits versus taxonomic, ecological and structural categories (no. parameters). Data are the Akaike Information Criteria (AIC) (adjusted R^2) degrees of freedom and *P*. AIC allows intra-row comparisons and models >20 above the minimum AIC have been removed.

Foliar variable	Species (14)	Life-form (7)	Strata (3)	Canopy (2)
%C	424 (0.51) 87****			452 (0.27) 99****
%N	134 (0.44) 87****	130 (0.43) 94****	146 (0.30) 98****	
C:N	733 (0.47) 87****	738 (0.41) 94****	752 (0.29) 98****	
$\delta^{13}C$	313 (0.36) 83****	309 (0.34) 90****		
$\delta^{15}N$				
Light saturation (*AQ*)	1356 (0.26) 86***	1372 (0.08) 93*	1369 (0.07) 97*	1368 (0.07) 98**
Light compensation (*AQ*)	563 (0.33) 86****	568 (0.26) 93****	563 (0.27) 97****	570 (0.21) 98****
Convexity (*AQ*)	508 (0.11) 87*	497 (0.15) 94**		
Respiration (*AQ*)	−16 (0.37) 86****	−3 (0.24) 93****	0 (0.18) 97****	6 (0.12) 98***
A_{max} (*AQ*), all	433 (0.53) 87****	479 (0.20) 94***		
V_{cmax} (AC_i)	668 (0.34) 84****	687 (0.15) 91**		
J_{max} (AC_i)	644 (0.23) 84***	652 (0.12) 91**		
TPU (AC_i)	328 (0.34) 84****	348 (0.14) 91**		
Convexity (induction %)	19 (0.34) 78****	37 (0.14) 85**		
IS50% (induction)	724 (0.31) 77****		740 (0.09) 88**	728 (0.19) 89****
WUE	369 (0.18) 80**			369 (0.08) 92**
SLA	928 (0.65) 81****	954 (0.51) 88****		
LMA	864 (0.59) 82****	887 (0.45) 89****		
N_{area}	99 (0.33) 81****	103 (0.26) 88****		
PNUE	882 (0.41) 81****	904 (0.20) 88***		
A_{mass}	926 (0.65) 82****	984 (0.32) 89****		
IS50%/A_{max}	487 (0.15) 77*			483 (0.08) 89**

Notes: See Appendix: Table A3 for an explanation of abbreviations. * $P < 0.05$; ** $P < 0.01$; *** $P < 0.001$; **** $P < 0.0001$. Status = invasive or native; Strata = low, mid or overstory position; Position = canopy or not; *M. polymorpha* = yes or no. Smartweed (*Persicaria punctata*) is not included in these analyses. The curve from which variables are calculated is provided in parenthesis following the variable name.

Table 5. General linear model results for leaf traits versus taxonomic, ecological and structural categories (no. parameters). Data are the Akaike Information Criteria (AIC) (adjusted R^2) degrees of freedom and *P*. AIC allows intra-row comparisons and models >20 above the minimum AIC have been removed.

Foliar variable	*M. polymorpha* (2)	Status (2)	Elevation (2)
%C			
%N			
C:N	747 (0.32) 99****		
$\delta^{13}C$			
$\delta^{15}N$		393 (0.14) 95***	376 (0.27) 95****
Light saturation (*AQ*)	1371 (0.04) 98*		1372 (0.03) 98*
Light compensation (*AQ*)	574 (0.17) 98****		
Convexity (*AQ*)	499 (0.09) 99**		
Respiration (*AQ*)	5 (0.14) 98****		
A_{max} (*AQ*), all		479 (0.17) 99****	
V_{cmax} (AC_i)			
J_{max} (AC_i)		653 (0.06) 96**	650 (0.09) 96**
TPU (AC_i)			
Convexity (induction %)	38 (0.08) 90**		
IS50% (induction)	742 (0.06) 89**	735 (0.13) 89***	737 (0.11) 89***
WUE			
SLA			
LMA			
N_{area}			
PNUE			
A_{mass}			
IS50%/A_{max}			480 (0.11) 89***

Notes: See Appendix: Table A3 for an explanation of abbreviations. * $P < 0.05$; ** $P < 0.01$; *** $P < 0.001$;**** $P < 0.0001$. Status = invasive or native; Strata = low, mid or overstory position; Position = canopy or not; *M. polymorpha* = yes or no. Smartweed (*Persicaria punctata*) is not included in these analyses. The curve from which variables are calculated is provided in parenthesis following the variable name.

Table 6. Best subsets models of leaf traits versus structural and modeled mean and standard deviation (SD) photosynthetic photon flux density (PPFD; $\mu mol \cdot m^{-2} \cdot s^{-1}$) and air temperature (°C). Data represents the *t*-ratio (*F*-ratio) and *P*-value significance, with increasing *, **, ***, ****, and ϕ representing *P*-values of 0.1, 0.05, 0.01, 0.001, and <0.0001, respectively. PPFD SD was not found significant for any leaf traits and not included in the table.

			Modeled variables	
Leaf traits	Elevation (m)	Leaf height (m)	PPFD mean	Air temp mean
%C		7.33 (53.78) ϕ		
%N		−4.15 (17.22) ϕ	1.81 (3.28)*	
C:N		5.01 (25.06) ϕ	−1.12 (1.25) NS	
$\delta^{13}C$				
$\delta^{15}N$		0.89 (0.7834) NS		6.15 (37.85) ϕ
Light saturation (*AQ*)		−2.2 (4.85)**	1.5 (2.24) NS	
Light compensation (*AQ*)	−1.84 (3.37)*	7.09 (50.26) ϕ		
AQE (×100)				
Convexity (*AQ*)		2.46 (6.06)**	2.69 (7.24)***	
Respiration (*AQ*)	1.75 (3.06)*	−3.72 (13.82)****		1.50 (2.25) NS
A_{max}†			5.63 (31.71) ϕ	1.69 (2.87) NS
V_{cmax} (AC_i)	2.89 (8.35)***	2.19 (4.78)**		4.51 (20.33) ϕ
J_{max} (AC_i)	2.36 (5.58)**	2.20 (4.82)**		3.98 (15.81) ϕ
TPU (AC_i)	2.10 (4.43)**			3.78 (14.29)****
Convexity (induction %)	2.12 (4.50)**	4.16 (17.31) ϕ	−1.71 (2.91)*	
IS50% (induction)	−2.58 (6.64)**	−4.27 (18.26) ϕ	1.76 (3.09)*	
WUE		3.24 (10.49)***	0.67 (0.45) NS	
SLA		−6.86 (47.03) ϕ	−1.77 (3.15)*	
LMA		6.74 (45.49) ϕ		
N_{area}		2.58 (6.66)**	3.00 (9.05)***	
PNUE		−2.85 (8.15)***	1.42 (2.01) NS	
A_{mass}		−4.70 (22.12) ϕ	2.09 (4.39)**	
IS50%/A_{max}		−3.04 (9.24)***	−3.31 (10.99)***	3.82 (14.59)****

Notes: See Appendix: Table A3 for an explanation of abbreviations. The curve from which variables are calculated is provided in parenthesis following the variable name.

† A_{max} values combined from light response and induction response curves.

0.03 ($P = 0.8741$) and 10.6 ($P = 0.0017$), respectively] (Appendix: Fig. A1). PCA axis three was not significantly correlated with MM-PPFD, MM-air temperature or any other spatial or structural variables.

K-means analysis of these axes revealed three distinct groups within the foliar dataset (Table 10 and Fig. 6), which following analysis were found to be sorted by growth light environment (Table 11). The low light cluster had lower maximum rates of photosynthesis (i.e., A_{max} and A_{mass}), including light saturation, but was able to reach A_{max} quickly as compared to the medium and high light clusters. Leaves in this cluster had higher leaf mass per area, foliar %C, and water use efficiency (WUE) and lower foliar %N, and photosynthetic nitrogen use efficiency (PNUE). The high light cluster had very high rates of A_{max} (and A_{mass}), PNUE, light saturation, triose phosphate utilization (TPU), V_{cmax}, and J_{max}. While many values were similar to other clusters, the medium light cluster was distinguished by intermediate values of A_{max}, A_{mass}, PNUE, induction response time (IS50%), and lower values of V_{cmax}, J_{max}, light compensation and saturation, and WUE. The medium light cluster had the lowest leaf mass per area.

We identified taxonomic, climatic and structural differences among the clusters (Table 11). The low light cluster was comprised of all tall plants with large DBH values whose sampled leaves occurred in low and less variable (i.e., low modeled standard deviation of PPFD) light environments. This cluster was composed entirely of native species and dominated by the dominant canopy species *M. polymorpha* and the understory tree fern *C. glaucum*. The medium light cluster was dominated by native species growing in light environments intermediate between the low- and high-modeled light clusters and often situated within the mid height strata. The high light cluster, similar in many respects to the medium light cluster, was composed of low height plants—the lowest strata

Table 7. Best subsets models of leaf traits versus structural and modeled mean and standard deviation (SD) photosynthetic photon flux density (PPFD; $\mu mol \cdot m^{-2} \cdot s^{-1}$) and air temperature (°C). Data represents the *t*-ratio (*F*-ratio) and *P*-value significance, with increasing *, **, ***, ****, and ϕ representing *P*-values of 0.1, 0.05, 0.01, 0.001, and <0.0001, respectively. PPFD SD was not found significant for any leaf traits and not included in the table.

Leaf trait	R^2	Adjusted R^2	*P*	*N*
%C	0.38	0.37	ϕ	101
%N	0.29	0.27	ϕ	97
C:N	0.31	0.30	ϕ	98
$\delta^{13}C$			NS	96
$\delta^{15}N$	0.29	0.28	ϕ	96
Light saturation (*AQ*)	0.13	0.11	****	95
Light compensation (*AQ*)	0.36	0.34	ϕ	98
AQE (×100)			NS	97
Convexity (*AQ*)	0.09	0.07	**	98
Respiration (*AQ*)	0.23	0.21	ϕ	97
A_{max}†	0.33	0.32	ϕ	186
V_{cmax} (AC_i)	0.28	0.25	ϕ	97
J_{max} (AC_i)	0.25	0.23	ϕ	98
TPU (AC_i)	0.22	0.21	ϕ	98
Convexity (induction %)	0.35	0.33	ϕ	90
IS50% (induction)	0.38	0.36	ϕ	89
WUE	0.12	0.10	***	93
SLA	0.36	0.35	ϕ	93
LMA	0.33	0.32	ϕ	96
N_{area}	0.11	0.09	***	93
PNUE	0.17	0.15	****	93
A_{mass}	0.35	0.33	ϕ	94
IS50%/A_{max}	0.18	0.16	****	89

Notes: See Appendix: Table A3 for an explanation of abbreviations. The curve from which variables are calculated is provided in parenthesis following the variable name.

† A_{max} values combined from light response and induction response curves.

of the forest—in high, but variable, modeled light environments. Composition of this cluster had abundant exotic species, including *H. gardnerianum* and *P. cattleianum*. It is likely that an additional cluster exists composed of top of canopy full sunlight *M. polymorpha* leaves. Our sampling effort did however include such leaves, but on *M. polymorpha* trees located in gaps or between taller individuals where rope traverses were feasible. It was not feasible in this study to sample leaves located at the top of canopy position in the tallest emergent individuals.

In general, leaves from any individual species were grouped in the same cluster (78 ± 18%; Table 2). A significant positive relationship between A_{max} (log-transformed) and mean modeled PPFD was found across the community the entire dataset (adjusted $R^2 = 0.25$, $P \leq 0.0001$, $N = 152$). However, individual clusters had different A_{max} to mean modeled PPFD relationships. No significant relationship existed for cluster one ($P = 0.2766$, $N = 152$), but a significant positive relationship existed for cluster two (adjusted $R^2 = 0.16$, $P \leq 0.0072$, $N = 44$) and cluster three (adjusted $R^2 = 0.26$, $P \leq 0.0040$, $N = 30$; Fig. 7).

Discussion

The main components of this project were performed as follows: (1) development of a two-dimensional map of LAI using airborne hyperspectral imagery; (2) derivation of a three-dimensional LAD map through integration of the two-dimensional LAI map with vertical profiles provided through airborne wLiDAR; (3) coding and validation of PAR and air temperature microclimate models integrating TOC climate measurements with forest structure from the LAD map; and (4) integrating modeled microclimate information with remote sensing and detailed field data to predict leaf traits and gas exchange dynamics for a suite of species occurring within a range of forest structural types (i.e., closed, open) along an elevation gradient.

Remote sensing

While passive and active remote sensing techniques have proven useful for large-scale analyses (Asner et al. 2005), remote sensing studies have historically been limited in their ability for finer scale analyses of ecosystem function. Recent advances have increased the capacity of remote sensing to integrate with ecosystems at scales appropriate for detailed functional analysis (Chambers et al. 2007). Space-borne hyperspectral imaging resulted in development of techniques to link remote sensing more directly to plant physiological traits (Asner et al. 2004, 2005). Airborne hyperspectral analysis provided finer spatial resolution studies, allowing detection of species composition and foliar properties (Carlson et al. 2007). Studies using large footprint LiDAR (Koetz et al. 2007) showed the utility of three-dimensional structural information, and airborne platforms have now integrated hyperspectral sensors with LiDAR systems (Asner et al. 2007). With this fusion,

Table 8. Predictors of Hapu'u (*Cibotium glaucum*) and Ohia (*Metrosideros polymorpha*) leaf traits. Data represent the slope (adjusted R^2) degrees of freedom and *P*-value of linear regressions. PPFD and air temp are modeled for each growth environment.

		Modeled variables	
Leaf traits	Leaf height (m)	PPFD mean	Air temp mean
A) *Metrosideros polymorpha*			
A_{max}†	NS	0.01 (0.13) 25*	NS
Light saturation†	NS	NS	NS
Day respiration†	NS	NS	NS
Convexity‡§	NS	NS	NS
IS50%‡	−0.56 (0.15) 20*	NS	NS
C:N	NS	NS	NS
$\delta^{13}C$	NS	NS	NS
$\delta^{15}N$	0.14 (0.13) 22*	NS	NS
B) *Cibotium glaucum*			
A_{max}†	−1.18 (0.26) 13*	0.02 (0.40) 13**	2.28 (0.61) 13***
Light saturation†	−179.25 (0.28) 13*	2.8 (0.34) 13*	345.79 (0.65) 13***
Day respiration†	0.11 (0.64) 12***	NS	NS
Convexity‡§	NS	NS	NS
IS50%‡	NS	0.12 (0.27) 12*	12.19 (0.35) 12*
C:N	NS	NS	NS
$\delta^{13}C$	NS	NS	NS
$\delta^{15}N$	NS	0.02 (0.27) 13 *	NS
C) Community			
A_{max}†	−0.14 (0.05) 97*	0.01 (0.26) 97****	1.67 (0.16) 97****
Light saturation†	−11.56 (0.05) 96*	0.49 (0.06) 96**	91.59 (0.06) 96**
Day respiration†	−0.02 (0.17) 96****	0 (0.04) 96*	NS
Convexity‡§	0.02 (0.08) 88**	NS	NS
IS50%‡	−1.11 (0.12) 87***	0.03 (0.04) 87*	8.22 (0.13) 87***
C:N	0.97 (0.18) 97****	−0.03 (0.08) 97**	NS
$\delta^{13}C$	NS	NS	NS
$\delta^{15}N$	NS	0.01 (0.13) 93***	1.55 (0.29) 93****

Note: See Appendix: Table A3 for an explanation of abbreviations.
† Calculated from light response curves.
‡ Calculated from inductance response curves.
§ Convexity of raw inductance data.
*$P < 0.05$; ** $P < 0.01$; *** $P < 0.001$;**** $P < 0.0001$.

simultaneous analysis of ecosystem structure and foliar traits has become feasible (Asner and Martin et al. 2008). There is now an increasing application of sensor fusion to elucidate forest properties at scales ranging from individual trees to global analyses (Todd et al. 2003, Reitberger et al. 2009, Zolkos et al. 2013).

A primary objective of many remote sensing studies has been to understand forest function in three dimensions spatially (Omasa et al. 2007). Efforts to better understand spatial properties of ecosystem dynamics, including productivity and canopy chemistry (Asner and Martin 2008), however, has been limited due to the difficulty of acquiring maps of forest interior structure and leaf area distribution (Houldcroft et al. 2005). In tropical forests especially, this difficulty has stemmed from the rapid extinction of the LiDAR signal in the dense overstory, and by the difficulties associated with collecting field parameterization and validation data within forest canopies (Laman 1995). Methods developed in this project have helped surmount some canopy access issues, in particular, intra-crown access using vertical transects off horizontal Tyrolean traverses.

Spatial resolution represents a serious obstacle to fully understanding forest dynamics. Interior forest light is known to be the primary limiter of photosynthesis in many tropical forests understories (Whitmore 1996). The distribution of foliage within a forest plays an integral role in light distribution (Chazdon et al. 1988, Chen et al. 1994, Montgomery 2004). Light that does reach the understory arrives as either direct or diffuse radiation, and global increases in diffuse radiation are predicted for the next 100 years (Mercado et al. 2009). Baldocchi and Wilson (2001) highlighted this importance through a modeling analysis which showed that differences

Table 9. Leaf trait principal component analysis (PCA) eigenvectors. PCA 1 and 2 have significant positive relationships with modeled mean photosynthetic photon flux density (μmol·m^{-2}·s^{-1}) and modeled mean air temperature (°C), respectively.

Foliar variable	PCA 1	PCA 2	PCA 3
%C	−0.126	0.273	0.117
%N	0.236	−0.279	0.215
C:N	−0.248	0.296	−0.0541
$\delta^{13}C$	−0.006	0.277	−0.074
$\delta^{15}N$	0.201	−0.063	0.040
Light saturation (AQ)	0.254	0.179	−0.322
Light compensation (AQ)	−0.246	0.179	−0.077
AQE (×100)	0.004	0.057	−0.349
Convexity (AQ)	−0.103	−0.080	0.419
Respiration (AQ)	0.244	−0.141	0.183
A_{max}†	0.326	0.178	−0.094
V_{cmax} (AC_i)	0.271	0.239	0.213
J_{max} (AC_i)	0.236	0.253	0.244
TPU (AC_i)	0.284	0.216	0.190
Convexity (induction %)	0.163	0.282	0.139
IS50% (induction)	0.078	−0.285	−0.153
WUE	−0.079	0.082	0.144
SLA	0.191	−0.269	−0.173
LMA	−0.183	0.310	0.140
N_{area}	0.110	−0.130	0.368
PNUE	0.281	0.173	−0.285
A_{mass}	0.341	0.074	−0.101

Notes: See Appendix: Table A3 for an explanation of abbreviations. The curve from which variables are calculated is provided in parenthesis following the variable name.

† A_{max} values combined from light response and induction response curves.

in leaf distribution throughout the forest vertical profile can alter forest net primary productivity (NPP) by up to 50%, largely through alteration of available PAR (Chazdon and Pearcy 1986*a*, *b*). Without an improved understanding of interactions between leaf area density distribution and light major errors will continue to exist in forest productivity models. However, no significant advances have been made in modeling 3D interior forest light dynamics at fine scales, although advances using medium-large footprint LiDAR are ongoing (Parker et al. 2001, Thomas et al. 2006). This has been due to several reasons including: (1) fine spatial scale of leaf area density determining direct light, and (2) the lack of a wLiDAR equipped remote sensing platform (Mallet and Bretar 2009) and decomposition algorithms (Wu et al. 2011) enabling detailed 3D analyses at a high spatial resolution. However, even field-based approaches have encountered difficulties and required inclusion of extensive stand structural information (Sonohat et al. 2004).

The development of the Carnegie Airborne Observatory integrating high pulse rate waveform LiDAR with a hyperspectral sensor has begun to overcome limitations to forest interior

Table 10. Leaf trait values (mean ± SD) for *K*-means low, medium and high modeled light clusters and results of among cluster one-way ANOVAs sorted by the adjusted R^2 value.

Leaf trait	Modeled light environment			Adjusted R^2	P
	Low	Medium	High		
Cluster size (N)	40	22	15		
A_{max} (AQ)	3.2 ± 1.2	3.4 ± 0.9	7.4 ± 1.7	0.64	<0.0001
A_{mass}	30.4 ± 13.2	55.4 ± 18.2	110.8 ± 42.7	0.64	<0.0001
PNUE	34.8 ± 15.8	45.2 ± 18.4	85 ± 30.3	0.47	<0.0001
LMA	108.8 ± 18.7	64.4 ± 16.6	77.3 ± 36.1	0.44	<0.0001
%C	47.8 ± 1.4	44.5 ± 1.9	45.6 ± 2.6	0.40	<0.0001
SLA	95 ± 18.7	166.2 ± 47	154.5 ± 65.7	0.40	<0.0001
Light saturation (AQ)	227.9 ± 157.6	221.8 ± 124.4	554.9 ± 225.4	0.37	<0.0001
C:N	40.2 ± 10.3	26.7 ± 6.8	27.1 ± 10.6	0.32	<0.0001
IS50% (induction)	8.3 ± 4.2	22.3 ± 13.9	26.2 ± 18.9	0.31	<0.0001
TPU (AC_i)	2 ± 1	1.7 ± 0.8	3.7 ± 1.6	0.30	<0.0001
%N	1.3 ± 0.3	1.9 ± 0.7	1.9 ± 0.6	0.27	<0.0001
V_{cmax} (AC_i)	12 ± 6.1	9.2 ± 4.3	20.5 ± 9.2	0.26	<0.0001
J_{max} (AC_i)	9.6 ± 5.2	6.9 ± 3.6	16.3 ± 9.2	0.23	<0.0001
Light compensation (AQ)	9.4 ± 3.8	5.7 ± 2.7	8.2 ± 3.3	0.17	0.0004
WUE	6.9 ± 1.6	5.2 ± 1.5	5.6 ± 1.9	0.15	0.0008
Respiration (AQ)	−0.5 ± 0.2	−0.4 ± 0.2	−0.5 ± 0.2	0.14	0.0017
Convexity (induction %)	0.5 ± 0.3	0.3 ± 0.2	0.4 ± 0.3	0.14	0.0017
$\delta^{13}C$	−30.2 ± 1.3	−31.1 ± 1.8	−30.1 ± 1.1	0.06	0.0427
$\delta^{15}N$	−2.8 ± 1.6	−2.8 ± 1.9	−2.3 ± 1.7	NS	NS
AQE (×100) (AQ)	6.8 ± 2.5	6.5 ± 0.9	6.7 ± 0.8	NS	NS
Convexity (AQ)	3.3 ± 3.2	2.6 ± 2.1	1.9 ± 1	NS	NS
N_{area}	1.4 ± 0.3	1.2 ± 0.7	1.3 ± 0.4	NS	NS

Notes: See Appendix: Table A3 for an explanation of abbreviations. The curve from which variables are calculated is provided in parenthesis following the variable name.

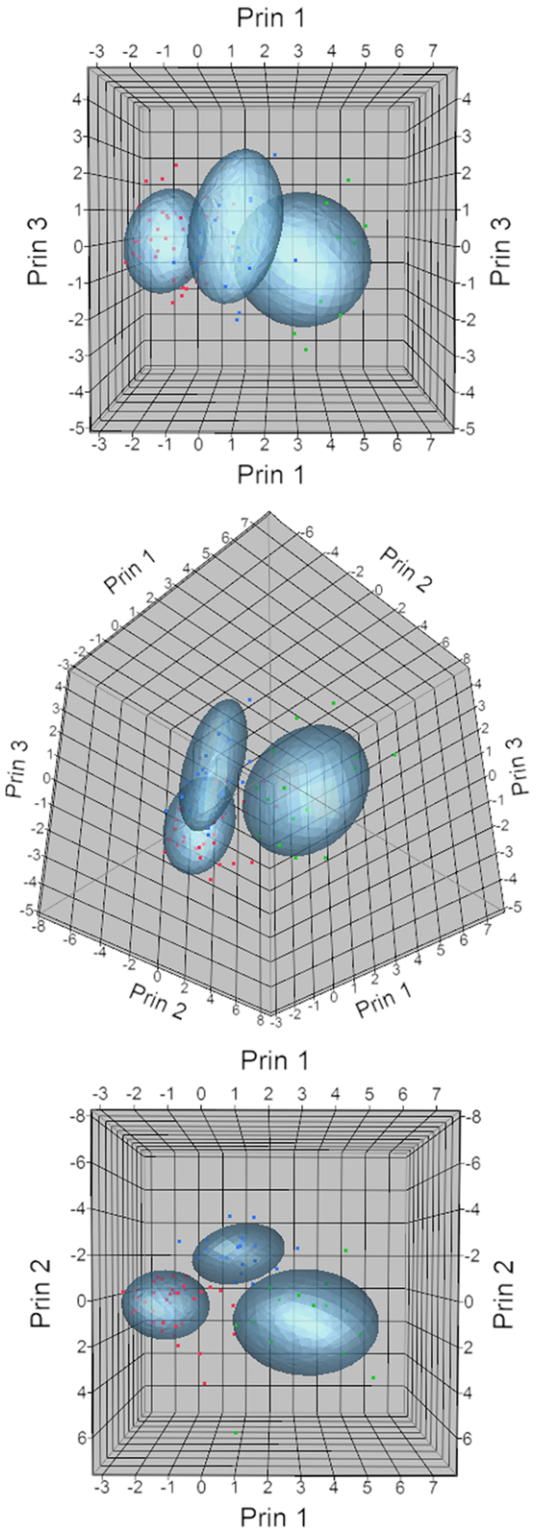

Fig. 6. Principal leaf trait clusters identified through *K*-means analysis. Low, medium and high light clusters are represented by the colors red, blue, and green, respectively.

microclimate modeling (Asner et al. 2007). The data collected for this study is among the highest spatial resolution available and allows us to test the feasibility of modeling microclimate dynamics at a temporal and spatial scale directly comparable to the scale of a leaf's growth environment. Future improvements to the PPFD and air temperature microclimate models we develop and parameterize in this study would include the use of interior forest PAR sensors distinguishing between direct and diffuse light and parameterization for other tropical forests with differing structure and gap dynamics (Kellner and Asner 2009). This would allow for an improved understanding of interactions between forest structure and the direct/diffuse light ratio versus the approach used in our study that combined direct and diffuse light as total PAR.

This study represents a development and validation step towards a rapid large-scale remote sensing based approach to model detailed forest productivity. Johnson and Smith (2006) have highlighted the need for such data. In addition, Alton et al. (2007) state that understanding how climate change will interact with plant photosynthesis is a key issue requiring further study. An approach built off an airborne system allows for rapid and economic collection of detailed forest structural measurements, and thereby models of microclimate and foliar ecophysiology, over a wide variety of forest types. Such efforts will enable a more unified understanding of climate change effects on the three-dimensional dynamics of forest photosynthesis and physiology at larger scales. For example, such information would be appropriate for integration with flux towers, which are providing significant insight into forest productivity dynamics (Schwalm et al. 2010).

Sources of leaf trait variation

Many factors influence a leaf's physiological traits, including: (1) structural parameters, such as the plant's height (Kenzo et al. 2006); and (2) site specific differences, such as general climate (Reich et al. 1996) or soil fertility (Ordoñez et al. 2009). Inter-species differences (Hikosaka 2004), result from divergent competitive growth strategies (Poorter et al. 2006) or simply life form (Wright et al. 2005), while intra-species occur as individual plants optimize their nutrient alloca-

Table 11. Forest elevation, structure and micro-climate values (mean ± SD) for low, medium and high light environment *K*-means clusters and results of among cluster one-way ANOVAs. Categorical classifications are % true and differences among clusters are assessed using the Pearson test.

Variable	Modeled light environment			Adjusted R^2	χ^2	*P*
	Low	Medium	High			
Cluster size (*N*)	40	22	15			
Elevation (m)	1176 ± 124	1173 ± 124	1090 ± 105	NS		NS
Canopy height (m)	21.6 ± 6.8	18.4 ± 8.2	21.1 ± 9.6	NS		NS
Total plant height (m)	12.8 ± 9.5	2.7 ± 2.4	2.6 ± 1.6	0.33		<0.0001
Leaf height (m)	7.5 ± 5.1	1.5 ± 0.5	1.8 ± 1.2	0.38		<0.0001
DBH (cm)	57.3 ± 59.7	9.3 ± 4.5	11.2 ± 2.7	0.26		<0.0001
Airborne LAI (m^2)	4.1 ± 0.3	4.1 ± 0.4	4.1 ± 0.3	NS		NS
Modeled mean PPFD ($\mu mol \cdot m^{-2} \cdot s^{-1}$)	173 ± 27.8	226 ± 94.5	318 ± 203.2	0.21		<0.0001
Modeled SD PPFD ($\mu mol \cdot m^{-2} \cdot s^{-1}$)	98 ± 14.4	121 ± 40.0	157 ± 75.5	0.21		<0.0001
Modeled mean temperature (°C)	16.9 ± 0.5	17 ± 0.7	17.6 ± 0.7	0.13		0.0018
Native spp. (%)	100	87	67		13.4	0.0013
M. polymorpha (%)	45	0	7		18.7	<0.0001
Canopy position (%)	78	42	7		44.4	<0.0001
Height strata: Upper (%)	53	27	0		33.5	<0.0001
Height strata: Middle (%)	40	43	47		...	...
Height strata: Lower (%)	8	30	53		...	...

tion to maximize productivity (Field and Mooney 1986, Hirose and Werger 1987, Hollinger 1989). The importance of vertical distributions in leaf traits, representing broad changes in micro-climate (Kumagai et al. 2001) and hydraulic limitations (Taylor and Eamus 2008), has been identified in many studies (Domingues et al. 2005). Leaves positioned in the upper canopy generally increase net CO_2 uptake while those situated in the lower canopy have reduced (or negative) uptake as the proportion of maintenance respiration costs are increased relative to C gain (Ellsworth and Reich 1993). Surprisingly, our analysis showed no correlation between leaf height and mean daily PPFD (Table 12). This difference is likely due to the forest structure in our study area, having a low LAI open canopy with dispersed tall relatively small DBH trees, differing from those in many tropical areas that have very high LAI canopies with heavily shaded forest interiors. Given this, horizontal differences in topography, low to mid-story leaf area, and gap dynamics may be dominant controls over microclimate variation, rather than vertical gradients as found in other studies in tropical forests (Domingues et al. 2005). A broad suite of leaf traits have been shown to co-vary, including positive relationships between foliar %N and A_{max} (Field and Mooney 1986, Reich et al. 1997), as we likewise find in this study (Appendix: Tables A1 and A2). This relationship partly results from the availability of photosynthetic enzymes limiting photosynthetic capacity (Field 1983). In addition to leaf N concentration and A_{max}, leaf photosynthetic induction rates, i.e., the activation and synthesis of photosynthesis related biochemical components and stomatal movements (Pearcy 1990) vary with both species and growth light environment (Bazzaz and Carlson 1982, Portes et al. 2008).

Species and structure

The single greatest source of leaf trait variation found in our study was inter-species differences (Table 4). Wright et al. (2004) used a global database of leaf traits, including 2,548 species, and found large variation among functional groups but strong co-variation among leaf traits, consistent with changes in species growth strategies along a continuous 'leaf economics spectrum' (Wright et al. 2004), constructing short lived, low LMA, high A_{max} leaves to long lived, high LMA, low A_{max} leaves. Likewise, Popma et al. (1992) found variation among species resulted from specialization to different growth environments, with gap-independent species producing nutrient poor leaves with low photosynthetic rates. In addition, they found that species adapted growing in a wide range of light environments show larger phenotypical plasticity in leaf traits. Markesteijn et al. (2007) also found leaf trait variation among 43 tropical forest

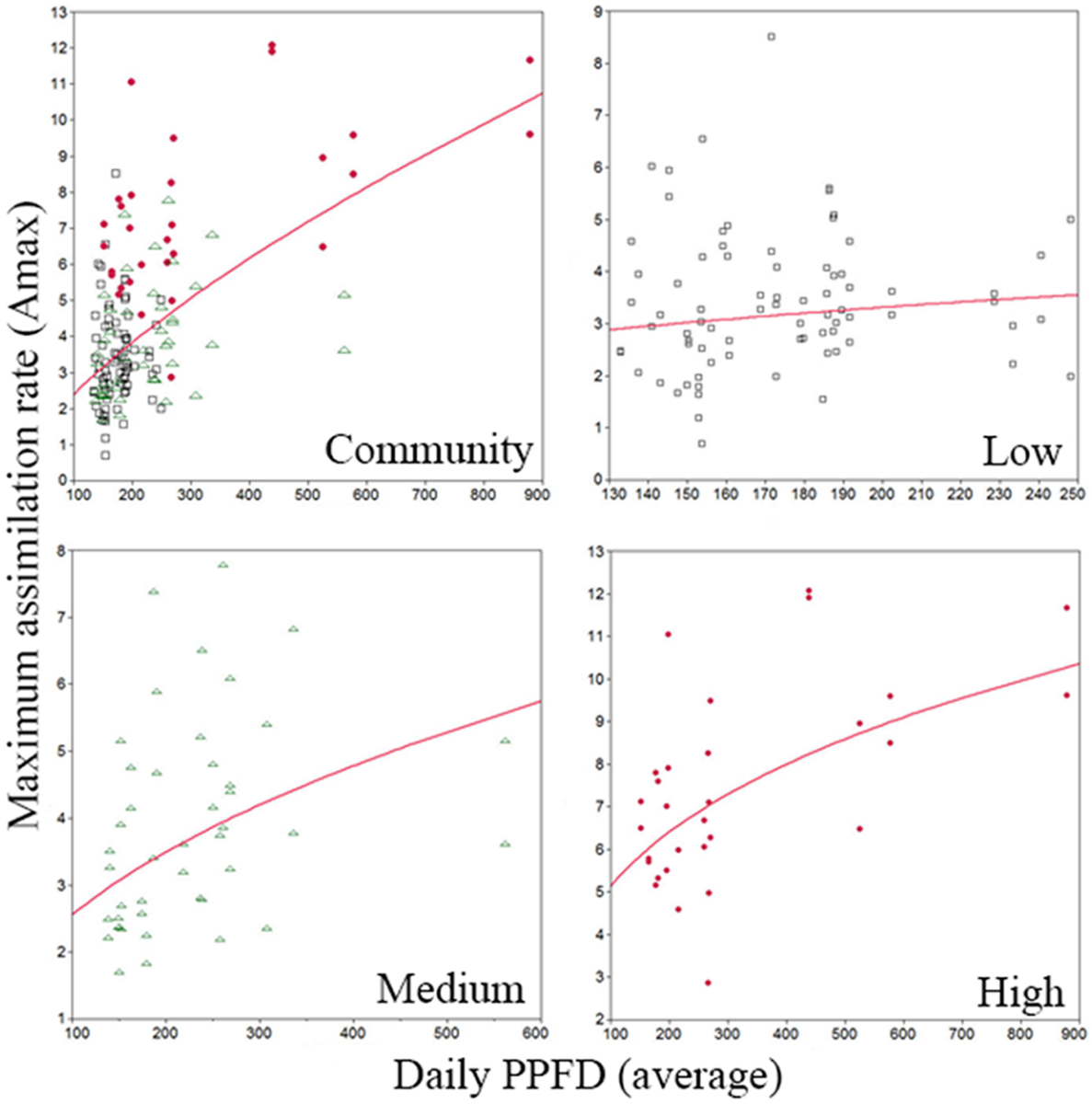

Fig. 7. Relationships (log-log regressions) between A_{max} (maximum CO_2 μmol·m^{-2}·s^{-1}) and modeled mean daily PPFD (μmol·m^{-2}·s^{-1}) for the entire community and modeled low, medium and high light leaf trait clusters. Regressions for the community and modeled medium and high light leaf trait clusters are significant ($P < 0.05$).

tree species to be dominated by inter-species differences, with short-lived pioneer species having the greatest leaf trait plasticity.

Many studies in Hawaii have focused on differences between species of exotic and native origin (Hughes and Denslow 2005). This topic is of conservation importance as many native ecosystems are undergoing invasion in which native dominated species composition becomes altered or dominated by exotic species, resulting in changes in composition, structure, and other ecological properties (Vitousek et al. 1987). Among other reasons, exotic species may invade native ecosystems following disturbance or when native communities have low resource use resulting in resource availability, termed the

Table 12. Pearson correlations between elevation and forest structure variables and modeled mean and standard deviation (SD) photosynthetic photon flux density (PPFD; $\mu mol \cdot m^{-2} \cdot s^{-1}$) and air temperature (°C). Only correlations having *P*-values < 0.05 are shown. * $P < 0.01$; ** $P < 0.001$. Row numbers refer to numbered column variables.

Variable	1	2	3	4	5	6	7	8
1. Elevation (m)								
2. Canopy height (m)	−0.56**							
3. Plant height (m)		0.27*						
4. Leaf height (m)		0.31*	0.93**					
5. Total canopy height (%)	0.28*	−0.22	0.79**	0.83**				
6. DBH (cm)			0.8**	0.82**	0.74**			
7. Modeled mean PPFD	−0.39**		−0.48**	−0.52**	−0.59**	−0.52**		
8. Modeled SD PPFD	−0.55**		−0.53**	−0.6**	−0.61**	−0.53**	0.85**	
9. Modeled mean air temperature	−0.92**	0.43	−0.21	−0.25	−0.42**	−0.32*	0.69**	0.76**

'fluctuating resource hypothesis' (Funk and Vitousek 2007). Funk and Vitousek (2007) studied the resource use efficiency (RUE) of invasive and native species and found that invasive species used limiting resources more efficiently, as indicated by higher photosynthetic rates (A_{max}), higher photosynthetic nitrogen use efficiency (PNUE), although water use efficiency (WUE) was not different. Asner et al. (2006) used remote sensing coupled with the CASA carbon cycle model and found that growth rates of *M. faya*, an invasive species, were 16–44% higher than *M. polymorpha*. In our study, exotic species exhibited significantly greater rates of photosynthesis and nutrient use, including higher foliar N and A_{max}. These findings are in line with other studies showing higher growth rates on non-resource limited sites, a reasonable assumption for our study area given the young age of the substrate. The lack of resource limitation is also exhibited in the non-significance of PNUE between our exotic and native species, a result found by Funk and Vitousek (2007).

Light and air temperature

Photosynthetic active radiation is a dominant limiting factor to total forest photosynthesis (Whitmore 1996, Kull 2002, Graham et al. 2003) and its availability plays a major role in survival, growth, ecology and physiology of forest plants (Chazdon and Pearcy 1986*a*, Myneni and Ganapol 1992), especially in the understory (Capers and Chazdon 2004). Photosynthetic active radiation dynamics vary greatly between forests of different stand architecture, even when species composition remains the same (Sonohat et al. 2004). In addition to light, air temperature is a primary determinant of photosynthesis and respiration (Berry and Bjorkman 1980) and increases in mean annual temperature (MAT) have been shown to correspond to increased total net primary productivity (Raich et al. 2006). We see the importance of these two environmental gradients expressed in our PCA analysis, with axis one being significantly correlated with modeled light and axis two correlated with modeled temperature. The fact that the first two axes encompass only 51% of the variability in leaf traits across our community may be partly explained by the exclusion of species, identified as a significant source of leaf trait variation, from the PCA. Preliminary analysis on our dataset does reveal the possibility of models with greater significance (PCA 1 vs. MM-PPFD; adjusted $R^2 = 0.58$, $P < 0.0001$, df = 77) and merits further investigation.

Differences in light and temperature in the plant growth environment are directly correlated with changes in leaf photosynthetic capacity, as well as a broad suite of ecophysiological characteristics (Wright et al. 2004, 2005). Field (1983) showed that plants optimize the distribution of N within their leaves according to the distribution of daily photosynthetic active radiation. Evans and Poorter (2001) found that photosynthesis was three times greater in ten dicotyledonous C_3 species grown under 1000 versus 200 $\mu mol \cdot m^{-2} \cdot s^{-1}$ PPFD, however photosynthesis per unit leaf dry mass was not significantly different due to increased specific leaf area (SLA) but constant nitrogen concentration. Hollinger (1989) showed that leaf N content and A_{max} followed vertical gradients according to available PPFD in the forest canopy. However, relation-

ships are not linear and photosynthesis of plants located in the understory often become light saturated at less than half of full sunlight intensity (Lambers et al. 1998). This may partly explain the low correlation we found between mean PPFD and light saturation at the community scale.

In our study, most leaf traits did follow vertical gradients, as shown by the significance of leaf height, but were also simultaneously correlated with light and air temperature; likely resulting from inconsistencies in the leaf height to PPFD relationship, which will be focus of future studies. Chazdon and Field (1987) found that in understory plants the light environment was only able to explain a maximum of 35.1% of the variation in A_{max}, indicating that other determinants, including climatic variation, topography or resource competition, were playing important roles. They also found that understory plants (versus plants growing in open gap environments) were less able to adjust A_{max} to variation in the light intensity of their growth environment, although compensation through increased light use efficiency was possible (Chazdon and Pearcy 1986*b*). Similar to their results, however, we found that modeled light variability did not significantly correlate to Amax, while simpler measures, such as canopy openness in their study, or in the case of our study modeled mean daily PPFD, did. This is similar to the percentage of variation in A_{max} explained for the *C. glaucum*, the dominant understory species in our study area. While direct radiation accounts for between 10 and 80% of total understory irradiance, and in some cases the majority of carbon fixation (Pearcy and Calkin 1983, Chazdon 1986, Pearcy 1990), it arrives to the understory of a forest within an intact canopy in the form of sun flecks lasting from seconds to minutes (Chazdon and Fletcher 1984). Thus, it is to the advantage of understory plants to develop the foliar capacity to rapidly use short temporal bursts of light (i.e., sunflecks) (Chazdon and Pearcy 1986*a*).

We found a positive correlation between modeled PPFD and time to reach 50% maximum assimilation rate (IS50%), differing from Rijkers et al. (2000), who found no differences in time to reach 90% maximum assimilation in spite of large differences in A_{max}. At first, this relationship appears to indicate that the dominant control over induction response time is the maximum photosynthetic rate of the leaf, although the Pearson correlation of 0.22 is low (Appendix: Table A1), and A_{max} is related to species differences and the illumination of the growth environment. However, further analysis shows that while A_{max} is related positively with growth environment, IS50% is more related to leaf height where it declines with height, although leaf height does have a significant negative correlation with modeled illumination environment. Given the low Pearson correlation, there is an opportunity to identify where leaves simultaneously maintain high maximum photosynthesis rates and rapid induction response times using the ratio of IS50%/A_{max}, which we consider a measure of induction response efficiency (i.e., lower values = more efficient). Our results show increasing induction response efficiency with increasing leaf height and in higher modeled light growth environments, but decreasing efficiency with increasing modeled air temperature. The relationship with increasing leaf height is logical as PPFD actually decreases at the base of the *M. polymorpha* canopy prior to increasing near the TOC. Decreasing efficiency in warmer environments also makes sense as increased availability of nutrients could results in reduced requirement for resource use optimization. As a plant likely shifts a range of leaf traits simultaneously, we expected to find a pattern of increasing WUE simultaneous to induction response efficiency. A linear regression analysis showed this significant negative relationship between them (adjusted $R^2 = 0.17$, $P \leq 0.0001$, $N = 90$), indicating simultaneous increases in light and water use efficiency. Similar to the findings of Funk and Vitousek (2007), we did not find significant differences in either water use efficiency or induction response efficiency between exotic and native species.

Stable isotopes

Foliar $\delta^{13}C$ is typically thought to represent changes in foliar water use efficiency (WUE) resulting from differences in water availability (Seibt et al. 2008) or structural differences in the leaf (Bonal et al. 2007). Variation in foliar $\delta^{13}C$ due to differences in atmospheric isotopic composition (i.e., increased respired versus atmospheric CO_2) would be unlikely to have an effect

higher than 3–5 m (Ometto et al. 2002) and leaf height was a non-significant predictor of variation in foliar $\delta^{13}C$. Our $\delta^{13}C$ values were similar to those reported in the Amazon (Ometto et al. 2006). However, for *M. polymorpha*, the canopy dominant in our study area, different conclusions regarding determinants of $\delta^{13}C$ variation have been found. Vitousek et al. (1990) found that, for Ohia (*M. polymorpha*), internal CO_2 resistance to diffusion resulting from increased LMA was a primary factor determining variation in $\delta^{13}C$, similar to the results found by Körner and Diemer (1987) who identified a pattern of increasing elevation, LMA, and $\delta^{13}C$. In addition, a positive relationship between increased carboxylation efficiency and leaf area based N content, associated with increasing elevation, was found to result in significantly less negative foliar $\delta^{13}C$ values (Cordell et al. 1999). Both studies agree that species differences is likely a primary factor determining $\delta^{13}C$, but is often overlooked during analysis, and Seibt et al. (2008) argues the potential for species differences in mesophyll conductance may mask trends in WUE. This is highlighted in our study, as only species differences (or as lumped into life-form groupings) were able to explain variation in foliar $\delta^{13}C$, with no correlations found between foliar $\delta^{13}C$ and any other leaf trait or predictor variable, including modeled mean PPFD or air temperature. As water is in abundant supply across the entire study area this result most likely represents maximized species variability when no potentially cofounding variation in water availability exists. We did find, however, that photosynthetic WUE increased significantly with increasing height in the canopy. We explain this as representing simultaneous increases in hydraulic limitations to water availability (Panek 1996) and shifts in species composition from fast growing less efficient species in the understory to, primarily, *M. polymorpha,* a slow growing canopy species with low photosynthetic capacity and high LMA (Cordell et al. 1999).

Foliar $\delta^{15}N$ represents an integrative measure of ecosystem dynamics over time (Adams and Grierson 2001), among other things. In our study, foliar $\delta^{15}N$ had no correlation with species but was significantly explained by air temperature. As decreasing foliar $\delta^{15}N$ is generally considered to represent a tightening of the N cycle (Austin and Vitousek 1998), the positive relationship between foliar $\delta^{15}N$ increasing with air temperature may indicate increased N availability at lower elevations resulting from faster nutrient cycling, including decomposition (Vitousek et al. 1989). This is further indicated by the lack of species significance and the significant multiple regression (adjusted $R^2 = 0.30$, $P \leq 0.0001$, df = 97) for foliar $\delta^{15}N$ which showed that leaf height was non-significant ($F = 0.69$, $P = 0.41$) while air temperature was highly significant ($F = 42.04$, $P \leq 0.0001$; see Fig. 8). These results are similar to those reported by Craine et al. (2009) and Amundson et al. (2003), who both reported a positive relationship between MAT and foliar $\delta^{15}N$. Foliar $\delta^{15}N$ values in our study were more depleted than those reported in parts of the Amazon (Ometto et al. 2006), similar to those reported by Martinelli et al. (1999) for *M. polymorpha*, but more negative than those reported by Cordell et al. (1999) which were collected at a different study site in Hawaii. This may be partly due to our study area having a comparatively young substrate, as compared to older substrates in the Amazon, and therefore a more conservative nitrogen cycle (Martinelli et al. 1999). Other sources of variation may include differences in rainfall (Austin and Vitousek 1998) or increased microbial activities at higher MAT (i.e., lower elevations) resulting in soil ^{15}N enrichment through the preferential loss of isotopically lighter N gases (Martinelli et al. 1999).

Clusters

Leaves may be stratified across light and temperature gradients due to changes in species composition based on each preferred growth environment or acclimation of individual leaves within a species (Reich et al. 1994). In our study area, simultaneous changes in species composition and leaf trait acclimation were evident. The community A_{max} to light relationship occurred in part due to transitions from low to medium to high light clusters of species (Reich et al. 1994). The response of each cluster differed however, similar to findings by Reich et al. (1998*a, b*), with those species growing in the highest light environments having significant correlations between light and A_{max}. Such differences are similar to those identified during forest succes-

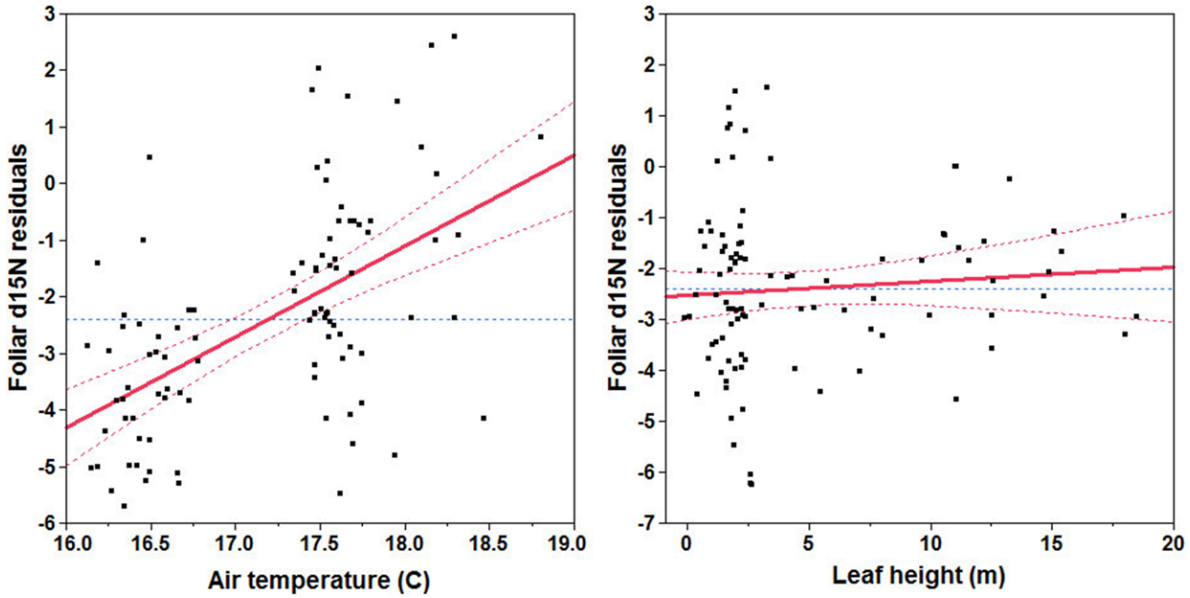

Fig. 8. Relationship of multiple regression foliar $\delta^{15}N$ residuals versus modeled mean daytime air temperature (°C) and leaf height (m).

sion, with shifts occurring from pioneer to climax species having differing capacities to acclimate to their irradiance growth environments (Poorter et al. 2006). Küppers et al. (1996) used both successional and light classes to show a reduction in the time to reach 50% induction state (IS50%) from pioneer through late successional species, but increasing time to reach IS50% with increasing light. Our results highlight that the acclimation capacity may differ regardless of the leaf trait cluster, based on mean values, to which a species is assigned. For example, *M. polymorpha*, a dominant overstory species, did not increase A_{max} with increases in light, while *C. glaucum* did. Ecologically, such changes make sense as species adapted to low light growth environments will require greater acclimation ability to take advantage of forest disturbances (Reich et al. 1994), i.e., including tree fall gaps, which result in large, but potentially short, increases in incident radiation both within the gaps and within the surrounding forest (Denslow et al. 1990).

Conclusions

We developed and validated a high-resolution three-dimensional model of microclimate through airborne wLiDAR hyperspectral fusion in a native dominated Hawaiian rainforest. Using this model, we show that a broad suite of leaf traits, occurring across species clusters, as well as within individual species, can be predicted by the modeled light and modeled air temperature of the growth environment. At the community scale, we show that correlations between A_{max} and light and air temperature of the growth environment changes with species clusters, as well as through acclimation of individuals leaves within a species to its unique growing environment. This relationship differs between species with different competitive growth strategies, with no acclimation occurring in the dominant overstory species *M. polymorpha*, but significant acclimation (i.e., plasticity) occurring in the dominant understory species *C. glaucum*. However, the greatest factor contributing to leaf trait variation was identified as inter-species variability. Analysis of stable isotopes shows that while foliar $\delta^{13}C$ is determined by inter-species differences (and in particular life form) in leaf physiology, foliar $\delta^{15}N$ is determined by ecosystem differences in nutrient cycling resulting from differences in MAT along the elevation gradient. While no significant differences in RUE were identified between exotic and native species, we did find that species in general increased their light and water RUE simultaneously related to

leaf height in general, the illumination state of their growth environment, and more broadly, to ecosystem changes in nutrient availability related to decreasing modeled air temperature associated with increasing elevation. The results of this study serve to develop and validate new tools useful for investigating ecosystem function at high spatial and temporal resolutions as well as provide insights into an ecosystem undergoing rapid degradation through species invasion and climate change. Future work built off this study will include full forest productivity modeling under different disturbance and climate change scenarios.

Acknowledgments

We give thanks to the following individuals for support in the lab and in the field and for their numerous insights during the course of this project: A. Wolf, A. Uowolo, B. Ostertag, B. Hwang, B. Paritosh, C. Williams, C. Lunch, D. Freyberg, D. Gelber, M. Gilbert, D. Leopold, E. Davidson, F. Inman-Narahari, F. Hughes, H. Farrington, H. Tidwell, J. Funk, J. Johnson, J. Kellner, J. Price, K. Brauman, K. Turbo, L. Fortini, M. Tweiten, P. Busby, P. Vitousek, R. Naesborg, R. Dirzo, S. Almeyda, T. Tobeck, J. Berry, J. Bingham, and G. Woods. We thank G. Priest, J. Broadbent, J. Mortimer, L. Pante, and M. Pante for support throughout. We thank the Burke family for assistance with field logistics. We give thanks to the staff of Department of Biology at Stanford University, Institute of Pacific Islands Forestry (IPIF) and the Hilo office of the Department of Forestry and Wildlife (DOFAW) for logistical support throughout. We thank Stanford University, the National Science Foundation (NSF), the Department of Energy (DOE), the National Aeronautics and Space Agency (NASA) and the Carnegie Institution for Science for financial support. We thank W. Clark, N. Dickson and M. Holbrook for help during the writing process. Analysis and writing was partially conducted while E. Broadbent was a doctoral and postdoctoral fellow and A. Almeyda Zambrano was a Giorgio Ruffolo Fellow in the Sustainability Science Program at Harvard University. Support from Italy's Ministry for Environment, Land and Sea is gratefully acknowledged. The Carnegie Airborne Observatory is made possible by the Gordon and Betty Moore Foundation, John D. and Catherine T. MacArthur, Grantham Foundation for the Protection of the Environment, Avatar Alliance Foundation, Margaret A. Cargill Foundation, W. M. Keck Foundation, Mary Anne Nyburg Baker and G. Leonard Baker Jr., and William R. Hearst III.

Literature Cited

Adams, M. A., and P. F. Grierson. 2001. Stable isotopes at natural abundance in terrestrial plant ecology and ecophysiology: an update. Plant Biology 3:299–310.

Alton, P. B., P. R. North, and S. O. Los. 2007. The impact of diffuse sunlight on canopy light-use efficiency, gross photosynthetic product and net ecosystem exchange in three forest biomes. Global Change Biology 13:776–787.

American Society of Civil Engineers. 2005. The ASCE standardized reference evapotranspiration equation. American Society of Civil Engineers, Reston, Virginia, USA.

Amundson, R., A. T. Austin, E. A. Schuur, K. Yoo, V. Matzek, C. Kendall, A. Uebersax, D. Brenner, and W. T. Baisden. 2003. Global patterns of the isotopic composition of soil and plant nitrogen. Global Biogeochemical Cycles 17:1031–1042.

Anderson, D. R. 2008. Model-based inference in the life sciences: a primer on evidence. Springer, New York, New York, USA.

Araujo, W. L., P. C. Dias, G. A. Moraes, E. F. Celin, R. L. Cunha, R. S. Barros, and F. M. DaMatta. 2008. Limitations to photosynthesis in coffee leaves from different canopy positions. Plant Physiology and Biochemistry 46:884–890.

Asner, G. P., K. M. Carlson, and R. E. Martin. 2005. Substrate age and precipitation effects on Hawaiian forest canopies from spaceborne imaging spectroscopy. Remote Sensing of Environment 98:457–467.

Asner, G. P., F. R. Hughes, T. A. Varga, D. E. Knapp, and T. Kennedy-Bowdoin. 2008*a*. Environmental and biotic controls over aboveground biomass throughout a tropical rain forest. Ecosystems 12:261–278.

Asner, G. P., R. F. Hughes, P. M. Vitousek, D. E. Knapp, T. Kennedy-Bowdoin, J. Boardman, R. E. Martin, M. Eastwood, and R. O. Green. 2008*b*. Invasive plants transform the three-dimensional structure of rain forests. Proceedings of the National Academy of Sciences 105:4519–4523.

Asner, G. P., D. E. Knapp, M. Jones, T. Kennedy-Bowdoin, R. E. Martin, C. B. Field, and J. Boardman. 2007. Carnegie airborne observatory: in-flight fusion of hyperspectral imaging and waveform light detection and ranging for three-dimensional studies of ecosystems. Journal of Applied Remote Sensing 1:013536.

Asner, G. P. and R. E. Martin. 2008. Spectral and chemical analysis of tropical forests: Scaling from leaf to canopy levels. Remote Sensing of Environment 112:3958–3970.

Asner, G. P., R. E. Martin, K. M. Carlson, U. Rascher, and P. M. Vitousek. 2006. Vegetation-climate interactions among native and invasive species in

Hawaiian rainforest. Ecosystems 9:1106–1117.

Asner, G. P., J. Mascaro, H. C. Muller-Landau, G. Vieilledent, R. Vaudry, M. Rasamoelina, J. S. Hall, and M. van Breugel. 2012. A universal airborne LiDAR approach for tropical forest carbon mapping. Oecologia 168:1147–1160.

Asner, G. P., D. Nepstad, G. Cardinot, and D. Ray. 2004. Drought stress and carbon uptake in an Amazon forest measured with spaceborne imaging spectroscopy. Proceedings of the National Academy of Sciences USA 101:6039–6044.

Aubin, I., M. Beaudet, and C. Messier. 2000. Light extinction coefficients specific to the understory vegetation of the southern boreal forest, Quebec. Canadian Journal of Forest Research 30:168–177.

Austin, A. T., and P. Vitousek. 1998. Nutrient dynamics on a precipitation gradient in Hawai'i. Oecologia 113:519–529.

Bai, K. D., D. B. Liao, and D. B. Jiang. 2008. Photosynthetic induction in leaves of co-occurring *Fagus lucida* and *Castanopsis lamontii* saplings grown in contrasting light environments. Trees: Structure and Function 22:449–462.

Baldocchi, D. D., and P. C. Harley. 1995. Scaling carbon dioxide and water vapour exchange from leaf to canopy in a deciduous forest: model testing and application. Plant Cell and Environment 18:1157–1174.

Baldocchi, D. D., and K. B. Wilson. 2001. Modeling CO_2 and water vapor exchange of a temperate broadleaved forest across hourly to decadal time scales. Ecological Modelling 142:155–184.

Bazzaz, F. A., and R. W. Carlson. 1982. Photosynthetic acclimation to variability in the light environment of early and late successional plants. Oecologia 54:313–316.

Berry, J., and O. Bjorkman. 1980. Photosynthetic response and adaptation to temperature in higher plants. Annual Review of Plant Physiology 31:491–543.

Boisvenue, C. and S. W. Running. 2006. Impacts of climate change on natural forest productivity—evidence since the middle of the 20th century. Global Change Biology 12:862–882.

Bonal, D., C. Born, C. Brechet, S. Coste, E. Marcon, J. C. Roggy, and J. M. Guehl. 2007. The successional status of tropical rainforest tree species is associated with differences in leaf carbon isotope discrimination and functional traits. Annals of Forest Science 64:169–176.

Boudreau, J., R. F. Nelson, H. A. Margolis, L. Guindon, and D. S. Kimes. 2008. Regional aboveground forest biomass using airborne and spaceborne LiDAR in Quebec. Remote Sensing of Environment 112:3876–3890.

Burnham, K. P., and D. R. Anderson. 2004. Multimodel inference: understanding AIC and BIC in model selection. Sociological Methods and Research 33:261–304.

Busby, P. E., P. Vitousek, and R. Dirzo. 2010. Prevalence of tree regeneration by sprouting and seeding along a rainfall gradient in Hawai'i. Biotropica 42:80–86.

Capers, R. S., and R. L. Chazdon. 2004. Rapid assessment of understory light availability in a wet tropical forest. Agricultural and Forest Meteorology 123:177–185.

Carlson, K. M., G. P. Asner, R. F. Hughes, R. Ostertag, and R. E. Martin. 2007. Hyperspectral remote sensing of canopy biodiversity in Hawaiian lowland rainforests. Ecosystems 10:536–549.

Chambers, J. Q., G. P. Asner, D. C. Morton, L. O. Anderson, S. S. Saatchi, F. D. Espirito-Santo, M. Palace, and C. Souza. 2007. Regional ecosystem structure and function: ecological insights from remote sensing of tropical forests. Trends in Ecology and Evolution 22:414–423.

Chazdon, R. L. 1986. Light variation and carbon gain in rain forest understorey palms. Journal of Ecology 74:995–1012.

Chazdon, R. L., and C. B. Field. 1987. Determinants of photosynthetic capacity in six rainforest Piper species. Oecologia 73:222–230.

Chazdon, R. L., and N. Fletcher. 1984. Photosynthetic light environments in a lowland tropical forest in Costa Rica. Journal of Ecology 72:553–564.

Chazdon, R. L., and R. W. Pearcy. 1986*a*. Photosynthetic responses to light variation in rainforest species. I. Induction under constant and fluctuating light conditions. Oecologia 69:517–523.

Chazdon, R. L., and R. W. Pearcy. 1986*b*. Photosynthetic responses to light variation in rainforest species: II carbon gain and photosynthetic efficiency during lightflecks. Oecologia 69:524–531.

Chazdon, R. L. and R. W. Pearcy. 1991. The importance of sunflecks for forest understory plants. BioScience 41:760–766.

Chazdon, R. L., K. Williams, and C. B. Field. 1988. Interactions between crown structure and light environment in five rain forest Piper species. American Journal of Botany 75:1459–1471.

Chen, S. G., B. Y. Shao, I. Impens, and R. Ceulemans. 1994. Effects of plant canopy structure on light interception and photosynthesis. Journal of Quantitative Spectroscopy and Radiative Transfer 52:115–123.

Cordell, S., G. Goldstein, F. C. Meinzer, and L. I. Jandley. 1999. Allocation of carbon and nitrogen in leaves of Metrosideros polymorpha regulates carboxylation capacity and $\delta^{13}C$ along an altitudinal gradient. Functional Ecology 13:811–818.

Cordell, S., G. Goldstein, D. Mueller-Dombois, D. Webb, and P. M. Vitousek. 1998. Physiological and morphological variation in *Metrosideros polymorpha*,

a dominant Hawaiian tree species, along an altitudinal gradient: the role of phenotypic plasticity. Oecologia 113:188–196.

Craine, J. M., A. J. Elmore, M. P. Aidar, M. Bustamante, T. E. Dawson, E. A. Hobbie, A. Kahmen, M. C. Mack, K. K. McLauchlan, A. Michelsen, G. B. Nardoto, L. H. Pardo, J. Peñuelas, P. B. Reich, E. A. Schuur, W. D. Stock, P. H. Templer, R. A. Virginia, J. M. Welker, and I. J. Wright. 2009. Global patterns of foliar nitrogen isotopes and their relationships with climate, mycorrhizal fungi, foliar nutrient concentrations, and nitrogen availability. New Phytologist 183:980–992.

Cramer, W., A. Bondeau, S. Schaphoff, W. Lucht, B. Smith, and S. Sitch. 2004. Tropical forests and the global carbon cycle: impacts of atmospheric carbon dioxide, climate change and rate of deforestation. Philosophical Transactions of the Royal Society 359:331–343.

Curtis, J. T., and R. P. McIntosh. 1951. An upland forest continuum in the prairie-forest border region of Wisconsin. Ecology 32:476–496.

Dang, Q. L., H. A. Margolis, M. Sy, M. R. Coyea, J. G. Collatz, and C. L. Walthall. 1997. Profiles of photosynthetically active radiation, nitrogen and photosynthetic capacity in the boreal forest: Implications for scaling from leaf to canopy. Journal of Geophysical Research 102:28845–28859.

Denslow, J. S., J. C. Schultz, P. M. Vitousek, and B. R. Strain. 1990. Growth responses of tropical shrubs to treefall gap environments. Ecology 71:165–179.

Dixon, R. K., S. Brown, R. A. Houghton, A. M. Solomon, M. C. Trexler, and J. Wisniewski. 1994. Carbon pools and the flux of global ecosystems. Science 263:185–190.

Domingues, T. F., J. A. Berry, L. A. Martinelli, J. P. Ometto, and J. R. Ehleringer. 2005. Parameterization of canopy structure and leaf-level gas exchange for an Eastern Amazonian Tropical Rain Forest. Earth Interactions 9:1–23.

Dubayah, R. O., S. L. Sheldon, D. B. Clark, M. A. Hofton, J. B. Blair, G. C. Hurtt, and R. L. Chazdon. 2010. Estimation of tropical forest height and biomass dynamics using lidar remote sensing at La Selva, Costa Rica. Journal of Geophysical Research 115:G00E09.

Ellsworth, D., and P. Reich. 1992. Leaf mass per area, nitrogen content and photosynthetic carbon gain in *Acer saccharum* seedlings in contrasting forest light environments. Functional Ecology 6:423–435.

Ellsworth, D., and P. Reich. 1993. Canopy structure and vertical patterns of photosynthesis and related leaf traits in a deciduous forest. Oecologia 96:169–178.

Evans, J. R. 1989. Photosynthesis and nitrogen relationships in leaves of C3 plants. Oecologia 78:9–19.

Evans, J. R., and H. Poorter. 2001. Photosynthetic acclimation of plants to growth irradiance: the relative importance of specific leaf area and nitrogen partitioning in maximizing carbon gain. Plant Cell and Environment 24:755–767.

Farquhar, G. D., S. V. Caemmerer, and J. A. Berry. 1980. A biochemical model of photosynthetic CO_2 assimilation in leaves of C3 species. Planta 149:78–90.

Field, C. B. 1983. Allocating leaf nitrogen for the maximization of carbon gain: leaf age as a control on the allocation program. Oecologia 56:341–347.

Field, C. B., M. J. Behrenfeld, J. T. Randerson, and P. Falkowski. 1998. Primary production of the biosphere: integrating terrestrial and oceanic components. Science 281:237–240.

Field, C. B., and H. A. Mooney. 1986. The photosynthesis–nitrogen relationship in wild plants. Pages 25–55 *in* T. Givnish, editor. On the economy of plant form and function. Cambridge University Press, Cambridge, UK.

Funk, J. L. and P. M. Vitousek. 2007. Resource-use efficiency and plant invasion in low-resource systems. Nature 446:1079–1081.

Gamon, J. A., and J. S. Surfus. 1999. Assessing leaf pigment content and activity with a reflectometer. New Phytologist 143:105–117.

Gastellu-Etchegorry, J., and V. Trichon. 1998. A modeling approach of PAR environment in a tropical rain forest in Sumatra: application to remote sensing. Ecological Modelling 108:237–264.

Gersonde, R., J. J. Battles, and K. L. O'Hara. 2004. Characterizing the light environment in Sierra Nevada mixed-conifer forests using a spatially explicit light model. Canadian Journal of Forest Research 34:1332–1342.

Giambelluca, T. W., Q. Chen, A. G. Frazier, J. P. Price, Y.-L. Chen, P.-S. Chu, J. Eischeid, and D. Delparte. 2011. The rainfall atlas of Hawai'i. http://rainfall.geography.hawaii.edu

Gitelson, A., and M. Merzlyak. 1996. Signature analysis of leaf reflectance spectra: Algorithm development for remote sensing of chlorophyll. Journal of Plant Physiology 148:495–500.

Graham, E., S. S. Mulkey, K. Kitajima, N. G. Phillips, and S. J. Wright. 2003. Cloud cover limits net CO_2 uptake and growth of a rainforest tree during tropical rainy seasons. Proceedings of the National Academy of Sciences 100:572–576.

Hansen, J., R. Ruedy, M. Sato, and K. Lo. 2010. Global surface temperature change. Reviews of Geophysics 48:1–29.

Hikosaka, K. 2004. Interspecific difference in the photosynthesis–nitrogen relationship: patterns, physiological causes, and ecological importance. Journal of Plant Research 117:481–494.

Hirose, T., and M. Werger. 1987. Maximizing daily canopy photosynthesis with respect to the leaf

nitrogen allocation pattern in the canopy. Oecologia 72:520–526.

Hirose, T., M. J. Werger, and J. W. van Rheenen. 1989. Canopy development and leaf nitrogen distribution in a stand of *Carex acutiformis*. Ecology 70:1610–1618.

Hollinger, D. Y. 1989. Canopy organization and foliage photosynthetic capacity in a broad-leaved evergreen montane forest. Functional Ecology 3:53–62.

Houldcroft, C. J., C. L. Campbell, I. J. Davenport, R. J. Gurney, and N. Holden. 2005. Measurement of canopy geometry characteristics using LiDAR laser altimetry: a feasibility study. IEEE Transactions on Geoscience and Remote Sensing 43:2270–2282.

Hudak, A. T., M. A. Lefsky, W. B. Cohen, and M. Berterretche. 2002. Integration of lidar and Landsat ETM+ data for estimating and mapping forest canopy height. Remote Sensing of Environment 82:397–416.

Hughes, R. F., and J. S. Denslow. 2005. Invasion by an N_2-fixing tree alters function and structure in wet lowland forests of Hawaii. Ecological Applications 15:1615–1628.

Hulme, M., and D. Viner. 1998. A climate change scenario for the tropics. Climatic Change 39:145–176.

Hunt, R., D. W. Hand, M. A. Hannah, and A. M. Neal. 1991. Response to CO_2 enrichment in 27 herbaceous species. Functional Ecology 5:410–421.

Johnson, D. M., and W. K. Smith. 2006. Low clouds and cloud immersion enhance photosynthesis in understory species of a southern Appalachian spruce-fir forest (USA). American Journal of Botany 93:1625–1632.

Kellner, J. R., and G. P. Asner. 2009. Convergent structural responses of tropical forests to diverse disturbance regimes. Ecology Letters 12:887–897.

Kenzo, T., T. Ichie, Y. Watanabe, R. Yoneda, I. Ninomiya, and T. Koike. 2006. Changes in photosynthesis and leaf characteristics with tree height in five dipterocarp species in a tropical rain forest. Tree Physiology 26:865–873.

Knohl, A., and D. D. Baldocchi. 2008. Effect of diffuse radiation on canopy gas exchange processes in a forest ecosystem. Journal of Geophysical Research 113:1–17.

Koetz, B., F. Morsdorf, G. Sun, K. Ranson, K. Itten, and B. Allgöwer. 2006. Inversion of a lidar waveform model for forest biophysical parameter estimation. IEEE Geoscience and Remote Sensing Letters 3:49–53.

Koetz, B., G. Sun, F. Morsdorf, K. Ranson, M. Kneubuhler, K. Itten, and B. Allgöwer. 2007. Fusion of imaging spectrometer and LIDAR data over combined radiative transfer models for forest canopy characterization. Remote Sensing of Environment 106:449–459.

Körner, C., and M. Diemer. 1987. In situ photosynthetic responses to light, temperature and carbon dioxide in herbaceous plants from low and high altitude. Functional Ecology 1:179–194.

Koukoulas, S., and G. A. Blackburn. 2004. Quantifying the spatial properties of forest canopy gaps using LiDAR imagery and GIS. International Journal of Remote Sensing 25:3049–3072.

Kull, O. 2002. Acclimation of photosynthesis in canopies: models and limitations. Oecologia 133:267–279.

Kumagai, T., K. Kuraji, H. Noguchi, Y. Tanaka, K. Tanaka, and M. Suzuki. 2001. Vertical profiles of environmental factors within tropical rainforest, Lambir Hills National Park, Sarawak, Malaysia. Journal of Forest Research 6:257–264.

Küppers, M., H. Timm, F. Orth, J. Stegemann, R. Stober, H. Schneider, K. Paliwal, K. S. Karunaichamy, and R. Ortiz. 1996. Effects of light environment and successional status on lightfleck use by understory trees of temperate and tropical forests. Tree Physiology 16:69–80.

Laisk, A., H. Eichelmann, V. Oja, B. Rasulow, E. Padu, I. Bichele, H. Pettai, and O. Kull. 2005. Adjustment of leaf photosynthesis to shade in a natural canopy: rate parameters. Plant, Cell and Environment 28:375–388.

Laman, T. G. 1995. Safety recommendations for climbing rain forest trees with ''single rope technique.'' Biotropica 27:406–409.

Lambers, H., F. S. Chapin, and T. L. Pons. 1998. Plant physiological ecology. Springer, New York, New York, USA.

Lim, K., P. Treitz, M. Wulder, B. St-Onge, and B. Flood. 2003. LiDAR remote sensing of forest structure. Progress in Physical Geography 27:88–106.

Liu, F., W. Yang, Z. Wang, Z. Xu, H. Liu, M. Zhang, Y. Liu, S. An, and S. Sun. 2010. Plant size effects on the relationships among specific leaf area, leaf nutrient content, and photosynthetic capacity in tropical woody species. Acta Oecologica 36:149–159.

Long, S. P., and C. J. Bernacchi. 2003. Gas exchange measurements, what can they tell us about the underlying limitations to photosynthesis? Procedures and sources of error. Journal of Experimental Botany 54:2393–2401.

Mallet, C., and F. Bretar. 2009. Full-waveform topographic lidar: State-of-the-art. ISPRS Journal of Photogrammetry and Remote Sensing 64:1–16.

Markesteijn, L., L. Poorter, and F. Bongers. 2007. Light-dependent leaf trait variation in 43 tropical dry forest tree species. American Journal of Botany 94:515–525.

Martin, R. E., and G. P. Asner. 2009. Leaf chemical and optical properties of *Metrosideros polymorpha* across environmental gradients in Hawaii. Biotropica

41:292–301.

Martinelli, L. A., M. C. Piccolo, A. R. Townsend, P. M. Vitousek, E. Cuevas, W. Mcdowell, G. P. Robertson, O. C. Santos, and K. Treseder. 1999. Nitrogen stable isotopic composition of leaves and soil: tropical versus temperate forests. Biogeochemistry 46:45–65.

Mazerolle, M. J. 2006. Improving data analysis in herpetology: using Akaike's Information Criterion (AIC) to assess the strength of biological hypotheses. Amphibia-Reptilia 27:169–180.

Meir, R., B. Kruijt, M. Broadmeadow, E. Barbosa, O. Kull, F. Carswell, A. Nobre, P. G. Jarvis, and P. Meir. 2002. Acclimation of photosynthetic capacity to irradiance in tree canopies in relation to leaf nitrogen concentration and leaf mass per unit area. Plant, Cell and Environment 25:343–357.

Mercado, L. M., N. Bellouin, S. Sitch, O. Boucher, C. Huntingford, M. Wild, and P. M. Cox. 2009. Impact of changes in diffuse radiation on the global land carbon sink. Nature 458:1014–1017.

Meyer, V., S. S. Saatchi, J. Chave, J. Dalling, S. Bohlman, G. A. Fricker, C. Robinson, and M. Neumann. 2013. Detecting tropical forest biomass dynamics from repeated airborne Lidar measurements. Biogeosciences Discuss 10:1957–1992.

Montgomery, R. 2004. Effects of understory foliage on patterns of light attenuation near the forest floor. Biotropica 36:33–39.

Mueller-Dombois, D. 1987. Natural dieback in forests. BioScience 37:575–583.

Mutua, F. M. 1994. The use of the Akaike Information Criterion in the identification of an optimum flood frequency model. Hydrological Sciences 39:235–244.

Myneni, R. B., and B. D. Ganapol. 1992. Remote sensing of vegetation canopy photosynthetic and stomatal conductance efficiencies. Remote Sensing of Environment 42:217–238.

Nozawa, T., S. Emori, A. Numaguti, Y. Tsushima, T. Takemura, T. Nakajima, A. Abe-Ouchi, and M. Kimoto. 2001. Projections of future climate change in the 21st century simulated by the CCSR/NIES CGCM under the IPCC SRES scenarios. Pages 15–28 *in* T. Matsuno and H. Kida, editors. Present and future of modelling global environmental change—toward integrated modelling. Terrapub, Tokyo, Japan.

Omasa, K., F. Hosoi, and A. Konishi. 2007. 3D lidar imaging for detecting and understanding plant responses and canopy structure. Journal of Experimental Botany 58:881–898.

Ometto, J. P., J. R. Ehleringer, T. F. Domingues, J. A. Berry, F. Y. Ishida, E. Mazzi, N. Higuchi, L. B. Flanagan, G. B. Nardoto, and L. A. Martinelli. 2006. The stable carbon and nitrogen isotopic composition of vegetation in tropical forests of the Amazon Basin, Brazil. Biogeochemistry 79:251–274.

Ometto, J. P., B. L. Flanagan, L. A. Martinelli, M. Z. Moreira, N. Higuchi, and J. R. Ehleringer. 2002. Carbon isotope discrimination in forest and pasture ecosystems of the Amazon Basin, Brazil. Global Biogeochemical Cycles 16:1–10.

Ordoñez, J. C., P. M. Bodegom, J. P. van Witte, I. J. Wright, P. B. Reich, and R. Aerts. 2009. A global study of relationships between leaf traits, climate and soil measures of nutrient fertility. Global Ecology and Biogeography 18:137–149.

Panek, J. 1996. Correlations between stable carbon-isotope abundance and hydraulic conductivity in Douglas-fir across a climate gradient in Oregon, USA. Tree Physiology 16:747–755.

Parker, G., M. Lefsky, and D. Harding. 2001. Light transmittance in forest canopies determined using airborne laser altimetry and in-canopy quantum measurements. Remote Sensing of Environment 76:298–309.

Pearcy, R. 1990. Sunflecks and photosynthesis in plant canopies. Annual Review of Plant Biology 41:421–453.

Pearcy, R. W., and H. Calkin. 1983. Carbon dioxide exchange of C_3 and C_4 tree species in the understory of a Hawaiian forest. Oecologia 58:19–25.

Poorter, L., L. Bongers, and F. Bongers. 2006. Architecture of 54 moist-forest tree species: traits, trade-offs, and functional groups. Ecology 87:1289–1301.

Poorter, L., and S. F. Oberbauer. 1993. Photosynthetic induction responses of two rainforest tree species in relation to light environment. Oecologia 96:193–199.

Popma, J., F. Bongers, and M. J. Werger. 1992. Gap-dependence and leaf characteristics of trees in a tropical lowland rain forest in Mexico. Oikos 63:207–214.

Portes, M. T., T. H. Alves, and G. M. Souza. 2008. Time-course of photosynthetic induction in four tropical woody species grown in contrasting irradiance habitats. Photosynthetica 46:431–440.

Potter, C. S., J. T. Randerson, C. B. Field, P. A. Matson, P. M. Vitousek, H. A. Mooney, and S. A. Klooster. 1993. Terrestrial ecosystem production: A process model based on global satellite and surface data. Global Biogeochemical Cycles 7:811–841.

R Development Core Team. 2013. R: A language and environment for statistical computing. R Foundation for Statistical Computing, Vienna, Austria.

Raich, J. W., A. E. Russell, K. Kitayama, W. J. Parton, and P. M. Vitousek. 2006. Temperature influences carbon accumulation in moist tropical forests. Ecology 87:76–87.

Reich, P. B., J. Oleksyn, and M. G. Tjoelker. 1996. Needle respiration and nitrogen concentration in Scots pine populations from a broad latitudinal

range: a common garden test with field grown trees. Functional Ecology 10:768–776.

Reich, P. B., D. S. Ellsworth, and M. B. Walters. 1998*a*. Leaf structure (specific leaf area) modulates photosynthesis-nitrogen relations: evidence from within and across species and functional groups. Functional Ecology 12:948–958.

Reich, P. B., D. S. Ellsworth, M. B. Walters, J. M. Vose, C. Gresham, J. C. Volin, and W. D. Bowman. 1999. Generality of leaf trait relationships: a test across six biomes. Ecology 80:1955–1969.

Reich, P. B., M. B. Walters, and D. S. Ellsworth. 1997. From tropics to tundra: global convergence in plant functioning. Proceedings of the National Academy of Sciences 94:13730–13734.

Reich, P. B., M. B. Walters, D. S. Ellsworth, and C. Uhl. 1994. Photosynthesis-nitrogen relations in Amazonian tree species. I. Patterns among species and communities. Oecologia 97:62–72.

Reich, P. B., M. B. Walters, D. S. Ellsworth, J. M. Vose, J. C. Volin, C. Gresham, and W. D. Bowman. 1998*b*. Relationships of leaf dark respiration to leaf nitrogen, specific leaf area and leaf life-span: a test across biomes and functional groups. Oecologia 114:471–482.

Reitberger, J., C. Schnörr, P. Krzystek, and U. Stilla. 2009. 3D segmentation of single trees exploiting full waveform LiDAR data. ISPRS Journal of Photogrammetry and Remote Sensing 64:561–574.

Rijkers, T., P. J. Vries, T. L. de Pons, and F. Bongers. 2000. Photosynthetic induction in saplings of three shade-tolerant tree species: comparing understory and gap habitats in a French Guiana rain forest. Oecologia 125:331–340.

Sampson, D. A., I. A. Janssens, and R. Ceulemans. 2006. Under-story contributions to stand level GPP using the process model SECRETS. Agricultural and Forest Meteorology 139:94–104.

Schwalm, C. R., C. A. Williams, K. Schaefer, A. Arneth, D. Bonal, N. Buchmann, J. Chen, B. E. Law, A. Lindroth, S. Luyssaert, M. Reichstein, and A. D. Richardson. 2010. Assimilation exceeds respiration sensitivity to drought: A FLUXNET synthesis. Global Change Biology 16:657–670.

Seibt, U., A. Rajabi, H. Griffiths, and J. A. Berry. 2008. Carbon isotopes and water use efficiency: sense and sensitivity. Oecologia 155:441–454.

Sellers, P., D. Randall, G. J. Collatz, J. A. Berry, C. B. Field, D. A. Dazlich, C. Zhang, G. D. Collelo, and L. Bounoua. 1996. A revised land surface parameterization (SiB2) for atmospheric GCMS. Part I: model formulation. Journal of Climate 9:676–705.

Sexton, J., T. Bax, P. Siqueira, J. Swenson, and S. Hensley. 2009. A comparison of LiDAR, radar, and field measurements of canopy height in pine and hardwood forests of southeastern North America. Forest Ecology and Management 257:1136–1147.

Sonohat, G., P. Balandier, and F. Ruchaud. 2004. Predicting solar radiation transmittance in the understory of even-aged coniferous stands in temperate forests. Annals of Forest Science 61:629–641.

Stadt, K. J., V. J. Lieffers, R. J. Hall, and C. Messier. 2005. Spatially explicit modeling of PAR transmission and growth of *Picea glauca* and *Abies balsamea* in the boreal forests of Alberta and Quebec. Canadian Journal of Forest Research 35:1–12.

Stone, C. P., L. W. Cuddihy, and J. T. Tunison. 1992. Responses of Hawaiian ecosystems to removal of feral pigs and goats. Pages 666–704 *in* C. P. Stone and J. M. Scott, editors. Alien plant invasions in native ecosystems of Hawaii. University of Hawaii Press, Honolulu, Hawaii, USA.

Taylor, D., and D. Eamus. 2008. Coordinating leaf functional traits with branch hydraulic conductivity: resource substitution and implications for carbon gain. Tree Physiology 28:1169–1177.

Thomas, V., D. Finch, J. McCaughey, T. Noland, L. Rich, and P. Treitz. 2006. Spatial modelling of the fraction of photosynthetically active radiation absorbed by a boreal mixedwood forest using a lidar–hyperspectral approach. Agricultural and Forest Meteorology 140:287–307.

Thomas, V., J. H. McCaughey, P. Treitz, D. A. Finch, T. Noland, and L. Rich. 2009. Spatial modelling of photosynthesis for a boreal mixedwood forest by integrating micrometeorological, LiDAR and hyperspectral remote sensing data. Agricultural and Forest Meteorology 149:639–654.

Todd, K. W., F. Csillag, and P. M. Atkinson. 2003. Three-dimensional mapping of light transmittance and foliage distribution using LiDAR. Canadian Journal of Remote Sensing 29:544–555.

Vitousek, P. M., G. P. Asner, O. A. Chadwick, and S. Hotchkiss. 2009. Landscape-level variation in forest structure and biogeochemistry across a substrate age gradient in Hawaii. Ecology 90:3074–3086.

Vitousek, P. M., C. B. Field, and P. A. Matson. 1990. Variation in foliar $\delta^{13}C$ in Hawaiian *Metrosideros polymorpha*: a case of internal resistance? Oecologia 84:362–370.

Vitousek, P. M., G. Shearer, and D. H. Kohl. 1989. Foliar $\delta^{15}N$ natural abundance in Hawaiian rainforest: patterns and possible mechanisms. Oecologia 78:383–388.

Vitousek, P. M., L. R. Walker, L. D. Whiteaker, D. Muller-Dombois, and P. M. Matson. 1987. Biological invasion by *Myrica faya* alters ecosystem development in Hawaii. Science 238:802–804.

Walters, M., and C. B. Field. 1987. Photosynthetic light acclimation in two rainforest *Piper* species with different ecological amplitudes. Oecologia 72:449–456.

Whitmore, T. C. 1996. A review of some aspects of

tropical rain forest seedling ecology with suggestions for further enquiry. Pages 3–39 *in* M. D. Swaine, editor. The ecology of tropical forest tree seedlings. Parthenon, Paris, France.

Wright, I. J., P. B. Reich, J. H. Cornelissen, D. S. Falster, E. Garnier, K. Hikosaka, B. B. Lamont, W. Lee, J. Oleksyn, N. Osada, H. Poorter, R. Villar, D. I. Warton, and M. Westoby. 2005. Assessing the generality of global leaf trait relationships. New Phytologist 166:485–496.

Wright, I. J., P. B. Reich, M. Westoby, D. D. Ackerly, Z. Baruch, F. Bongers, J. Cavender-Bares, T. Chapin, J. H. Cornelissen, M. Diemer, J. Flexas, E. Garnier, P. K. Groom, J. Gulias, K. Hikosaka, B. B. Lamont, T. Lee, W. Lee, C. Lusk, J. J. Midgley, M. L. Navas, U. Niinemets, J. Oleksyn, N. Osada, H. Poorter, P. Poot, L. Prior, V. I. Pyankov, C. Roumet, S. C. Thomas, M. G. Tjoelker, E. J. Veneklaas, and R. Villar. 2004. The worldwide leaf economics spectrum. Nature 428:821–827.

Wu, J., J. van Aardt, J. McGlinchy, and G. P. Asner. 2011. A robust signal processing chain for small-footprint waveform LiDAR. IEEE Transactions on Geoscience and Remote Sensing 99:1–14.

Zolkos, S. G., S. J. Goetz, and R. Dubayah. 2013. A meta-analysis of terrestrial aboveground biomass estimation using lidar remote sensing. Remote Sensing of Environment 128:289–298.

Supplemental Material

Appendix

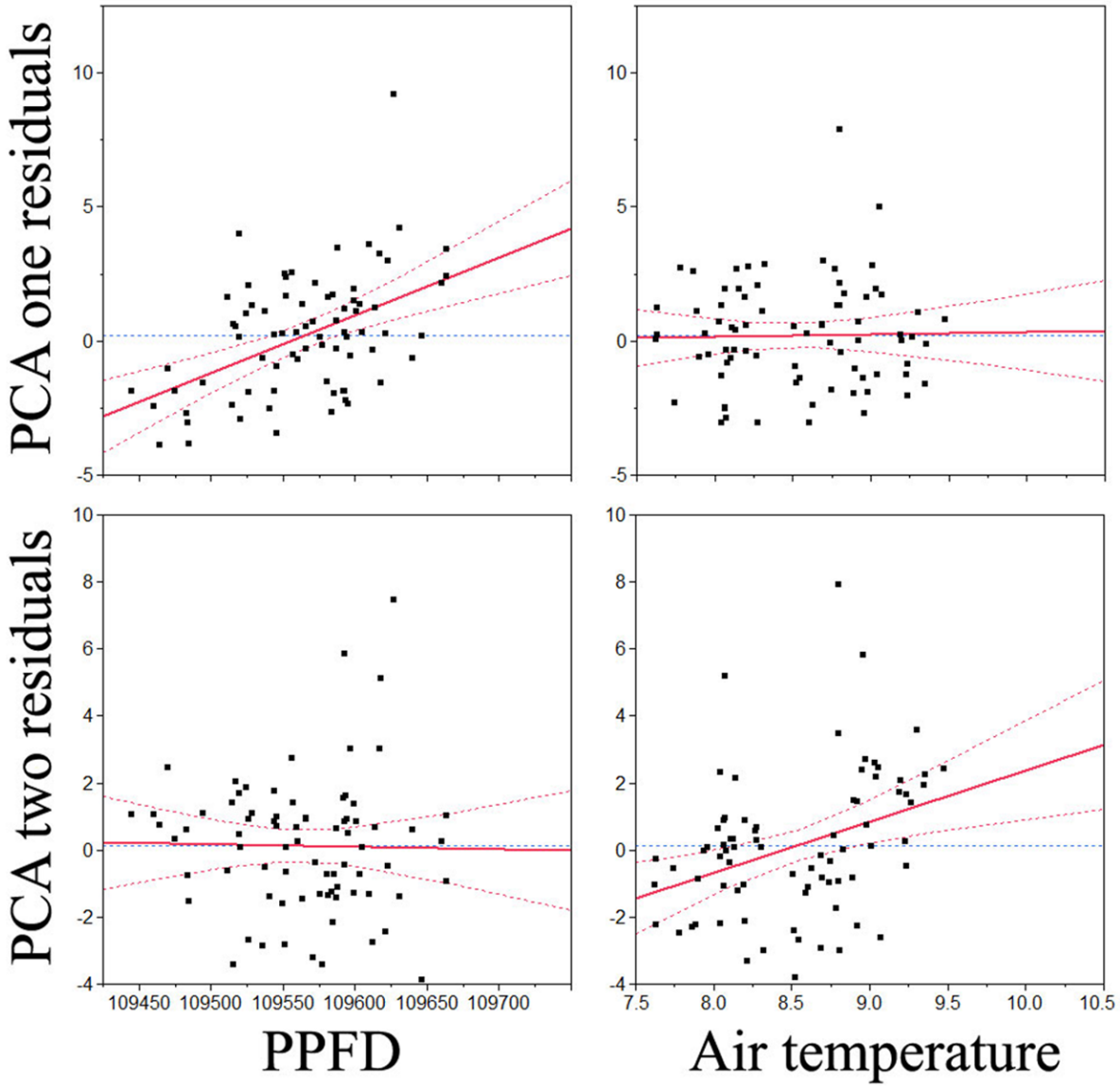

Fig. A1. Relationships between multiple regression residuals of axis one and two of principal component analysis (PCA) of foliar ecophysiological variables versus box-cox transformed modeled mean photosynthetic photon flux density ($\mu mol \cdot m^{-2} \cdot s^{-1}$) and modeled mean air temperature (°C).

Table A1. Pearson correlations between foliar variables 1–10. Only correlations having *P*-values < 0.05 are shown. *P*-values < 0.01, < 0.001, and < 0.0001 are represented by *, **, and ϕ, respectively. Column heading numbers correspond to numbered variables in the first column.

Variable	1	2	3	4	5	6	7	8	9	10
1. C%										
2. N%	−0.24									
3. C:N	0.37**	−0.87ϕ								
4. $\delta^{13}C$										
5. $\delta^{15}N$		0.31*	−0.29*							
6. Light saturation (*AQ*)		0.27*	−0.32*		0.28*					
7. Light compensation (*AQ*)	0.41ϕ	−0.36**	0.38**			−0.22				
8. Convexity (*AQ*)						−0.50ϕ				
9. Respiration (*AQ*)	−0.36**	0.35**	−0.36**				−0.86ϕ			
10. A_{max} (*AQ*)		0.39ϕ	−0.37**		0.35**	0.85ϕ	−0.25	−0.26*	0.29*	
11. V_{cmax} (AC_i)		0.29*	−0.21		0.27*	0.45ϕ				0.69ϕ
12. J_{max} (AC_i)		0.24			0.23	0.37**				0.61ϕ
13. TPU (AC_i)		0.30*	−0.22		0.28*	0.48ϕ				0.73ϕ
14. Convexity (induction %)	0.23					0.27*				0.43ϕ
15. IS50% (induction)	−0.55ϕ	0.28*	−0.3*		0.29*	0.21				0.22
16. WUE	0.40ϕ									
17. SLA	−0.41ϕ	0.44ϕ	−0.51ϕ				−0.32*		0.25	
18. LMA	0.45ϕ	−0.51ϕ	0.59ϕ				0.42ϕ		−0.37**	
19. N_{area}		0.53ϕ	−0.36**		0.3*					
20. PNUE	−0.33*					0.65ϕ	−0.25	−0.29*	0.21	0.77ϕ
21. A_{mass}	−0.26	0.51ϕ	−0.5ϕ		0.27*	0.69ϕ	−0.31*	−0.23	0.32*	0.87ϕ

Notes: See Table A3 for an explanation of abbreviations. The curve from which variables are calculated is provided in parenthesis following the variable name.

Table A2. Pearson correlations between foliar variables 11–20. Only correlations having *P*-values <0.05 are shown. *P*-values <0.01, <0.001, and <0.0001 are represented by *, **, and ϕ, respectively. Column heading numbers correspond to numbered variables in the first column here and in Table A1.

Variable	11	12	13	14	15	16	17	18	19	20
12. J_{max} (AC_i)	0.98ϕ									
13. TPU (AC_i)	0.98ϕ	0.95ϕ								
14. Convexity (induction %)	0.41ϕ	0.37**	0.39**							
15. IS50% (induction)				−0.5ϕ						
16. WUE				0.32*	−0.46ϕ					
17. SLA										
18. LMA							−0.92ϕ			
19. N_{area}	0.22	0.23	0.21				−0.45ϕ	0.42ϕ		
20. PNUE	0.43ϕ	0.36**	0.49ϕ	0.26	0.34**		0.53ϕ	−0.47ϕ	−0.4ϕ	
21. A_{mass}	0.56ϕ	0.46ϕ	0.61ϕ	0.33*	0.36**		0.60ϕ	−0.56ϕ		0.84ϕ

Note: See Table A3 for an explanation of abbreviations.

Table A3. Glossary of selected abbreviations as used in this study.

Abbreviation	Description of variable
A	Net CO_2 assimilation rates
AC_i	Normalized CO_2 response curves
AGB	Aboveground biomass
AIC	Akaike Information Criteria
A_{mass}	Ratio of A_{max} to unit leaf dry mass
A_{max}	Maximum photosynthesis capacity
AQ	Normalized light response curves
AQE	Apparent quantum efficiency
CAO	Carnegie Airborne Observatory
C_i	Intracellular CO_2 concentration
CV	Total coefficient of variation
D	Density
DBH	Diameter at breast height
Do	Dominance
F	Frequency
GPS	Geographic positioning system
HiFIS	High-fidelity hyperspectral imager
IDL	Interactive Data Language
IS	Induction state
IS50%	Time to reach 50% maximum assimilation rate
IV	Importance value
J_{max}	Maximum rate of RuBP regeneration
LAI	Leaf area index
LiDAR	Light detection and ranging
LMA	Leaf mass per area
MAT	Mean annual temperature
MM	Modeled mean
mNDVI	Modified red edge normalized difference vegetation index
N_{area}	Nitrogen content per area
PAR	Photosynthetic active radiation
PCA	Principal component analyses
PNUE	Photosynthetic nitrogen use efficiency
PPFD	Photosynthetic photon flux density
Q	Incident PPFD
RUE	Resource use efficiency
SLA	Specific leaf area
TOC	Top of canopy
TPU	Triose phosphate utilization
V_{cmax}	Maximum rate of carboxylation by Rubisco
wLiDAR	Waveform light detection and ranging
WUE	Water use efficiency

SUPPLEMENT

R scripts for conducting clear sky PAR simulations described in the main text (*Ecological Archives* C005-006-S1).